Motor learning requires myelination to reduce asynchrony and spontaneity in neural activity

Kato, Daisuke ; Wake, Hiroaki ; Lee, Philip R. ; Tachibana, Yoshihisa ; Ono, Riho ; Sugio, Shouta ; Tsuji, Yukio ; Tanaka, Yasuyo H. ; Tanaka,…

(Citation)
Glia,68(1):193-210

(Issue Date)
2020-01

(Resource Type)
journal article

(Version)
Version of Record

Received: 26 March 2018 | Revised: 23 July 2019 | Accepted: 12 August 2019

DOI: 10.1002/glia.23713

GLIA

WILEY

RESEARCH ARTICLE

Motor learning requires myelination to reduce asynchrony and spontaneity in neural activity

Daisuke Kato[1,2,3,4] | Hiroaki Wake[1,2,4,5,11] | Philip R. Lee[6] | Yoshihisa Tachibana[4] | Riho Ono[4] | Shouta Sugio[4] | Yukio Tsuji[4] | Yasuyo H. Tanaka[2,7] | Yasuhiro R. Tanaka[2,7] | Yoshito Masamizu[2,7] | Riichiro Hira[2] | Andrew J. Moorhouse[8] | Nobuaki Tamamaki[9] | Kazuhiro Ikenaka[10] | Noriyuki Matsukawa[3] | R. Douglas Fields[6] | Junichi Nabekura[1,11,12] | Masanori Matsuzaki[2,7,11,12]

[1]Division of Homeostatic Development, National Institute for Physiological Sciences, Okazaki, Japan

[2]Division of Brain Circuits, National Institute for Basic Biology, Okazaki, Aichi, Japan

[3]Department of Neurology, Graduate School of Medicine, Nagoya City University, Nagoya, Japan

[4]Division of System Neuroscience, Kobe University Graduate School of Medicine, Kobe, Japan

[5]Precursory Research for Embryonic Science and Technology, Japan Science and Technology Agency, Saitama, Japan

[6]Section on Nervous System Development and Plasticity, National Institutes of Health, National Institute of Child Health and Human Development, Bethesda, Maryland

[7]Department of Physiology, Graduate School of Medicine, The University of Tokyo, Tokyo, Japan

[8]Department of Physiology, School of Medical Sciences, The University of New South Wales, Sydney, Australia

[9]Department of Morphological Neural Science, Graduate School of Medical Sciences, Kumamoto University, Kumamoto, Japan

[10]Division of Neurobiology and Bioinformatics, National Institute for Physiological Sciences, Okazaki, Japan

[11]Core Research for Evolutional Science and Technology, Japan Science and Technology Agency, Saitama, Japan

[12]School of Life Science, The Graduate School for Advanced Study, Hayama, Japan

Correspondence
Hiroaki Wake, Division of System Neuroscience, Kobe University Graduate School of Medicine, 7-5-2 Kusunoki-cho, Chuo-ku, Kobe 650-0017, Japan.
Email: hirowake@med.kobe-u.ac.jp
Masanori Matsuzaki, Department of Physiology, Graduate School of Medicine, University of Tokyo, Hongo, Bunkyo-ku, Tokyo 113-0033, Japan.
Email: mzakim@m.u-tokyo.ac.jp

Funding information
Japan Agency for Medical Research and Development, Grant/Award Number: JP17dm0107053; Japan Science and Technology Agency, Grant/Award Number: JPMJCR1755; Ministry of Education, Culture, Sports, Science and Technology, Grant/Award Numbers: 18H02598, Grants-in-Aid for Scientific Research, Grants-in-Aid for Scientific Research on Innovativ, Grants-in-Aid for Young Scientists (A)

Abstract

Myelination increases the conduction velocity in long-range axons and is prerequisite for many brain functions. Impaired myelin regulation or impairment of myelin itself is frequently associated with deficits in learning and cognition in neurological and psychiatric disorders. However, it has not been revealed what perturbation of neural activity induced by myelin impairment causes learning deficits. Here, we measured neural activity in the motor cortex during motor learning in transgenic mice with a subtle impairment of their myelin. This deficit in myelin impaired motor learning, and was accompanied by a decrease in the amplitude of movement-related activity and an increase in the frequency of spontaneous activity. Thalamocortical axons showed variability in axonal conduction with a large spread in the timing of postsynaptic cortical responses. Repetitive pairing of forelimb movements with optogenetic stimulation of thalamocortical axon terminals restored motor learning. Thus, myelin regulation helps to maintain the synchrony of cortical spike-time arrivals through long-range axons, facilitating the propagation of the

information required for learning. Our results revealed the pathological neuronal circuit activity with impaired myelin and suggest the possibility that pairing of noninvasive brain stimulation with relevant behaviors may ameliorate cognitive and behavioral abnormalities in diseases with impaired myelination.

KEYWORDS
axonal conduction, calcium imaging, motor learning, myelination, neuron–glia interactions, oligodendrocyte, optogenetics

1 | INTRODUCTION

Myelin formation by oligodendrocytes surrounding axons in the central nervous system regulates conduction velocity (CV), which is a key component of fast and efficient information processing in the brain (Emery, 2010; Fields, 2008; Nave, 2010). Myelinated long-range axons form white matter and transmit information between many cortical and subcortical gray matter regions. Human studies using magnetic resonance imaging (MRI) have shown that white matter plasticity is associated with motor learning (Scholz, Klein, Behrens, & Johansen-Berg, 2009; Zatorre, Fields, & Johansen-Berg, 2012). In the mouse, motor learning or motor behavioral improvements require proliferation and differentiation of oligodendrocyte precursor cells (OPCs) in the white matter and motor cortex (Gibson et al., 2014; McKenzie et al., 2014; Xiao et al., 2016). A pharmacological block of action potentials in the retina inhibits proliferation of OPCs in optic nerves (Barres & Raff, 1993). Electrical stimulation of medullary pyramids (Li, Brus-Ramer, Martin, & McDonald, 2010) and optogenetic stimulation of cortical layer 5 (L5) excitatory neurons (Gibson et al., 2014) promotes the differentiation of OPCs. Inhibition of vesicular release from neurons to mature oligodendrocytes impairs myelination, both in vitro (Wake et al., 2015; Wake, Lee, & Fields, 2011) and in vivo (Hines, Ravanelli, Schwindt, Scott, & Appel, 2015; Mensch et al., 2015). These results indicate that neuronal activity regulates myelination through OPCs and mature oligodendrocytes and thus impairment of activity-dependent myelination or myelin itself may contribute on learning deficits. Given that distinct myelinated long-range axons input to a common cell or circuit, appropriate regulation of the CVs is assumed to help synchronization of these distinct neural inputs (Pajevic, Basser, & Fields, 2014; Roelfsema, Engel, Konig, & Singer, 1997). An assembly of time-locked inputs would consolidate information processing by inducing spike-timing-dependent plasticity (STDP) between optimally myelinated axons and their postsynaptic neurons, or in the local cortical circuit (Feldman, 2012; Nave, 2010; Veniero, Ponzo, & Koch, 2013). This is believed to promote the formation of the cortical ensemble required for behavioral learning.

Impaired regulation of myelination or impairment of myelin itself frequently accompanies learning deficits, cognitive dysfunction, and aging (Bennett & Madden, 2014; Liu et al., 2012; Makinodan, Rosen, Ito, & Corfas, 2012;McKenzie et al., 2014 ; Xiao et al., 2016). In MRI using diffusion tensor imaging, white matter changes are frequently observed in dementia and considered as one of the earliest signs of cognitive decline (Amlien & Fjell, 2014; Back et al., 2011). Genome-wide analysis reveals differential expression of myelination-related genes in schizophrenia (Hakak et al., 2001). Genetic deletion of myelin regulatory factor causes deficient maturation of OPCs in mature mice, resulting in impaired motor learning (McKenzie et al., 2014; Xiao et al., 2016). Social isolation impairs adult myelination in the mouse prefrontal cortex and causes behavioral deficits (Liu et al., 2012; Makinodan et al., 2012). Although it has been reported that impaired myelin regulation increases the conduction time of myelinated axons in vivo (Bando et al., 2008; Tanaka, Ikenaka, & Isa, 2006), it is poorly understood how this impairs cortical circuit properties that are relevant to learning and cognition. At a single neuron level, cortical activity is high in mice models of Alzheimer's disease (Busche et al., 2008), fragile X syndrome (Goncalves, Anstey, Golshani, & Portera-Cailliau, 2013), and Rett syndrome (Zhang, Peterson, Beyer, Frankel, & Zhang, 2014), and in these mice models, the abnormalities in cortical neuronal activity are associated with defects in inhibition. It is unknown whether a mouse model of impaired myelination shows similar properties.

Here, we hypothesize that impaired myelin disrupts cortical neuronal activity and results in impaired motor learning. As disrupting myelination can have widespread and severe consequences, including inflammation, as seen in the debilitating demyelination disorders and leukodystrophies (Saugier-Veber et al., 1994), an animal model with slight deficits in CV and learning, but without apparent histological or motor deficits, is suitable for testing this hypothesis. Transgenic mice with extra copies of the myelin proteolipid protein 1 gene (PLP-tg mice [Kagawa et al., 1994]) have reduced CV in spinal ascending and descending tracts at 2 months of age, including the pyramidal tract (Tanaka et al., 2006) due to thinner myelin thickness (Tanaka et al., 2009) and abnormal processes of oligodendrocytes (Shimizu et al., 2013). PLP-tg mice also exhibit some impairment of learning and behavior at the same age, although neither histological demyelination nor motor deficits are apparent (Tanaka et al., 2006; Tanaka et al., 2009). In this study, we used PLP-tg mice at 2 months of age and a forelimb movement learning task to test our hypothesis. We focused on the primary motor cortex (M1), as the proliferation and differentiation of M1 OPCs is accelerated, and the activity of M1 cortical neurons dynamically changes during motor learning (Huber et al., 2012; Masamizu et al., 2014; McKenzie et al., 2014; Peters, Chen, & Komiyama, 2014;

Xiao et al., 2016). We performed two-photon Ca^{2+} imaging, electrical recording, and optogenetics to identify the abnormalities in M1 activity in these mice. Then, we demonstrated that the repetitive pairing of forelimb movements with synchronous activation of thalamocortical axon terminals was able to restore learning.

2 | MATERIALS AND METHODS

2.1 | Animals and head plate fixation surgery

All experiments were approved by the Institutional Animal Care and Use Committee of the National Institutes of Natural Sciences and the Institutional Animal Care and Use Committee of Kobe University Graduate School of Medicine. The animals were given free access to food and water in a 12 hr light/dark cycle. For experiments with virus injections, 6-week-old male hemizygous PLP-tg mice (BDF1 background) (Kagawa et al., 1994; Tanaka et al., 2009) and parvalbumin (PV)-Cre mice (C57BL/6 background) (Tanahira et al., 2009) were anesthetized by intraperitoneal injection of ketamine (74 mg/kg) and xylazine (10 mg/kg). Prior to surgery, the skin was disinfected with 70% alcohol and the skull was exposed and cleaned, and a head plate was firmly attached with dental cement (Fuji luto BC; GC, Tokyo, Japan, Bistite II; Tokuyama Dental, Tokyo, Japan). The surface of the intact skull was subsequently coated with acrylic-based dental adhesive resin cement (Super bond; Sun Medical, Shiga, Japan) to avoid drying, as previously described (Masamizu et al., 2014). Mice were allowed to recover for 1 day before virus injection. Up to five animals were kept together in a cage before the head plate was attached. After surgery, mice were housed singly to avoid damage to the head plate and the glass window.

2.2 | AAV surgery and injection

Adeno-associated virus (AAV) was injected 2–3 weeks before imaging. Dexamethasone sodium phosphate (1.32 mg/kg) and carprofen (6 mg/kg) were administered intraperitoneally 1 hr before surgery to prevent cerebral edema and inflammatory response, respectively. Under 1% isoflurane anesthesia, a ~2 mm diameter circular craniotomy (circle centered at ~0.2 mm anterior and ~1 mm lateral from bregma) was performed over the left primary motor cortex (M1; circle centered ~0.2 mm anterior and ~1 mm lateral from bregma), as previously described (Masamizu et al., 2014). A total of 1 μl recombinant AAV (rAAV2/1-Syn-GCaMP3: 2.76×10^{13} vector genomes/ml or rAAV2/1-CAG-flex-GCaMP6f: 1.35×10^{13} vector genomes/ml, UPenn Vector Core) solution was injected through a glass pipette (tip diameter, 25–30 μm) connected to a picospritzer into layer 2/3 (L2/3) of the left M1. The pipette was then maintained in place for an additional 10 min. After the injection, 3% (w/v) agarose L (Nippon Gene, Tokyo, Japan) was placed over the craniotomy, a 4.5 mm diameter glass coverslip (Matsunami Glass, Osaka, Japan) was pressed onto the agarose surface, and the edges were sealed with dental cement and dental adhesive resin cement. Mice were then returned to their cages. Postoperative care included water supplemented with the antibiotics sulfadiazine (24 mg/kg) and trimethoprim (4.8 mg/kg), and daily carprofen (6 mg/kg, ip).

2.3 | Self-initiated lever-pull task

The voluntary (self-initiated) forelimb movement task was modified from a previously described procedure (Hira et al., 2013; Masamizu et al., 2014). Mice with head plates were habituated to the task device for 1 hr per day for 2 days before the start of the experiment. The mice were inserted into a body chamber and their head was fixed by placing the head plate between holders attached to a stage. After habituation, mice were water-deprived in their home cages and maintained at 85% of their normal body weight throughout the experiments. Each mouse was trained to perform the voluntary right-forelimb movement for 1 hr per day for 12 training days. When mice pulled the lever by 5 mm and held it there for 600 ms, they were rewarded with a 4 μL drop of water from a spout near their mouths. The lever was then quickly returned to the wait position by a solenoid valve. The lever could not be moved again from the wait position for 1 s. After this immobilization period, mice were allowed to pull the lever again. If a lever pull failed to be held for the full 600 ms (i.e., a failed trial), the lever was not immobilized and the mice were allowed to again pull the lever at any time. A program written in LabVIEW (National Instruments, Austin, TX) was used to control the timing of the reward, the lever return, and the immobilization of the lever, and continuously monitor the lever position. Mouse behavior and performance was monitored with an infrared video camera. Mice were allowed ad libitum access to 1 ml water following each training session. For Figure 1b–d, 20 wild-type (WT) mice (10 with and 10 without AAV transduction) and 19 PLP-tg mice (9 with and 10 without AAV transduction) were used.

2.4 | Two-photon imaging

Two-photon images were acquired from the left M1 during performance of the lever-pull task (on Days 1, 3, 5, 7, and 9) using either an FV1000-MPE microscope (Olympus, Tokyo, Japan) with a ×25 objective (XLPlan, NA 1.05; Olympus) and a mode-locked Ti:sapphire laser (MaTai HP; Spectra Physics, CA) at a wavelength of 910–920 nm, or an LSM 7 MP system (Zeiss, Jena, Germany) with a ×20 objective (XLPlan, NA 1.0; Zeiss) and a mode-locked Ti:sapphire Chameleon Ultra II laser (Coherent, Santa Clara, CA) tuned to 920 nm. Fluorescence was collected with GaAsP photomultiplier tubes (Hamamatsu Photonics, Shizuoka, Japan). Laser intensity was 20–40 mW. The imaged fields were 508.93×508.93 μm at 150–200 μm depth below the cortical surface. Pixel size was 1.988 μm. Frame duration was 420 ms. Continuous 1,000-frame imaging was repeated in each field for 10–30 min. The lever position and solenoid signal were recorded simultaneously with the Ca^{2+} imaging. Two-photon imaging in WT/PV-Cre and PLP-tg/PV-Cre mice was performed on Day 1.

2.5 | Image analysis

Analyses were performed with an ImageJ plug-in (1.37v; NIH) and scripts written in MATLAB (version 7; MathWorks, Natick, MA). Movies were corrected for focal plane displacements (X, Y, and rotation-angle shifts) as previously described (Hira et al., 2013; Masamizu et al., 2014). Fields in which motion artifacts remained after correction and crowded fields were removed. The outlines of the cell-based regions of interest (ROIs) were determined using a semi-automated algorithm based on maximization of the correlation coefficients of the intensities of nearby pixels over time, along with cell sizes and shapes, and were confirmed by visual inspection (Masamizu et al., 2014). The numbers of analyzed ROIs were as follows: WT mice (five fields from five mice on each day), 97 on Day 1, 143 on Day 3, 107 on Day 5, 141 on Day 7, and 188 on Day 9; PLP-tg mice (five fields from five mice on each day), 125 on Day

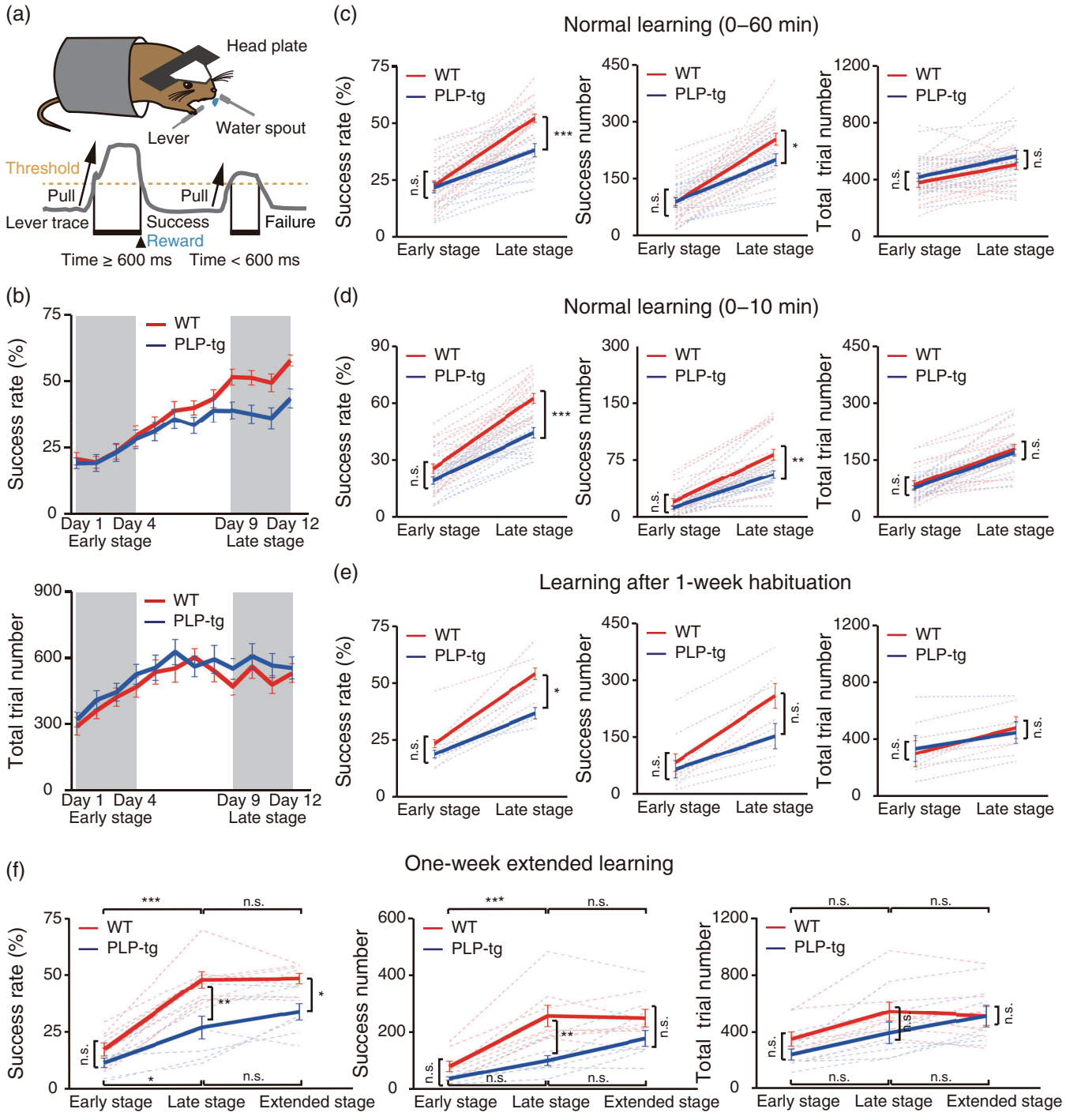

FIGURE 1 Legend on next page

1, 203 on Day 3, 213 on Day 5, 240 on Day 7, and 199 on Day 9. The numbers of analyzed PV-positive ROIs were as follows: WT mice, 115 (five fields from four mice); PLP-tg mice, 145 (nine fields from five mice). The fluorescence within each ROI was averaged, and background fluorescence was subtracted from this average value. Ca^{2+} transients were defined according to the method in a previous report (Eto et al., 2011). All frames were divided into a sequence of segments with monotonically increasing fluorescence values that started at the initial time point and finished at the end time point. For each segment, when the increase in the fluorescence value from the initial to end time points was more than fourfold the *SD* of the 35th percentile of total fluorescence, one Ca^{2+} transient was assigned to the end time point. We then defined the task-related Ca^{2+} transient as the time point existing 1.2 s before the start point of successful lever pulling behavior and 1.6 s after the start point of successful lever pulling behavior. Imaging sessions with more than three successful lever pulls were analyzed. If the time point of a Ca^{2+} transient was outside of the period from 1.2 s before the start point of any lever pull to 1.6 s after the start point of any lever pull, it was defined as a spontaneous Ca^{2+} transient.

2.6 | In vivo electrophysiology

Sixteen-channel silicone probes with 177 μm^2 recording sites (NeuroNexus Technologies, Ann Arbor, MI) spaced 25 μm apart at depths of 500–600 μm below the cortical surface were used to record L2/3 and L5 neuronal activity in the left M1 in 8–9-week-old mice. All in vivo recordings were acquired using the Omniplex system (Plexon, Dallas, TX). Spike signals were filtered at a bandpass of 300 Hz to 8 kHz. Spikes were detected by threshold-level crossing, generally set at 50 μV, and sorting of single units was carried out using principal component analysis in an offline sorter (Plexon). In L2/3, 68 units from 10 awake WT mice, 63 units from 10 anesthetized WT mice, 56 units from 13 awake PLP-tg mice, and 51 units from 12 anesthetized PLP-tg mice were recorded. In L5, 55 units from nine awake WT mice, 55 units from nine anesthetized WT mice, 58 units from nine awake PLP-tg mice, and 58 units from nine anesthetized PLP-tg mice were recorded. In the CNQX experiment, 10 units were recorded from four PLP-tg mice.

2.7 | Optogenetic stimulation of thalamic neurons

A total of 500 nl AAV2/1-Syn-ChR2 (H134R)-EYFP (2.11×10^{13} vector genomes/ml, UPenn Vector Core) was injected into the left thalamus (1 mm posterior and 1 mm lateral from the bregma, and 3.2 mm below the pia). After 2–3 weeks of virus injection, electrophysiological experiments with optogenetic stimulation were performed using planar electrodes under 0.8–1% isoflurane anesthesia to reduce behavioral effects in the awake state. For optogenetic stimulation of thalamic afferents in the cortex, the fiber-optic cable was placed close to the cortical surface that had been exposed by the craniotomy. For optogenetic stimulation of the thalamus, a fiber-optic cable (~500 μm diameter) was acutely implanted at the same coordinates as the thalamic viral injection but at a depth of 2.2 mm. Then, 20 × 20 ms pulses of a 470 nm LED (Lumencor, Beaverton, OR) were delivered at 1 Hz to elicit responses. The power at the fiber-optic tip was approximately 4 mW. Units that showed a stable (at least one) response to every optogenetic stimulation were recorded, and spikes that occurred within 50 ms after the onset of the stimulation were analyzed.

FIGURE 1 Changes in task performance during learning of a lever-pull task. (a) Schematic of the lever-pull task. Head-restrained mice were trained to perform self-initiated right-forelimb movements. A 600 ms lever pull was required to receive a drop of water. (b) Time course of the 60 min-averaged lever-pull success rate (upper) and the 60 min-averaged number of total trials (lower) in WT (red) and PLP-tg mice (blue). (c) Success rate (left), number of successful trials (center) and number of total trial lever pulls (right) in early (Days 1–4) and late (Days 9–12) training stages in the WT (red, $n = 20$) and PLP-tg (blue, $n = 19$) mice shown in plot b. Success rate: $F_{1,74} = 10.79$, $p = .99$ (early), $p = 2.1 \times 10^{-4}$ (late), two-way ANOVA followed by Tukey's test. Success number: $F_{1,74} = 3.56$, $p = 1.00$ (early), $p = .036$ (late), two-way ANOVA followed by Tukey's test. Total trial number: $F_{1,74} = 1.86$, $p = .86$ (early), $p = .67$ (late), two-way ANOVA followed by Tukey's test. Data are presented as the mean ± *SEM*. *$p < .05$, ***$p < .001$, n.s.: nonsignificant. (d) Success rate (left), number of successful trials (center), and number of total trials (right) during the initial 10 min session in early (Days 1–4) and late (Days 9–12) training stages in the WT (red, $n = 20$) and PLP-tg (blue, $n = 19$) mice shown in plot b. Success rate: $F_{1,74} = 24.15$, $p = .29$ (early), $p = 1.1 \times 10^{-5}$ (late), two-way ANOVA followed by Tukey's test. Success number: $F_{1,74} = 10.78$, $p = .75$ (early), $p = .0028$ (late), two-way ANOVA followed by Tukey's test. Total trial number: $F_{1,74} = 0.65$, $p = .95$ (early), $p = .93$ (late), two-way ANOVA followed by Tukey's test. Data are presented as the mean ± *SEM*. **$p < .01$, ***$p < .001$, n.s.: nonsignificant. (e) Success rate (left), number of successful trials (center) and number of total trials (right) in early (Days 1–4) and late (Days 9–12) sessions after 1 week of habituation to the experimental apparatus. Five WT mice (red) and five PLP-tg mice (blue) were used. Success rate: $F_{1,16} = 6.96$, $p = .86$ (early), $p = .043$ (late), two-way ANOVA followed by Tukey's test. Success number: $F_{1,16} = 2.79$, $p = .99$ (early), $p = .22$ (late), two-way ANOVA followed by Tukey's test. Total trial number: $F_{1,16} = 0.00$, $p = .99$ (early), $p = .99$ (late), two-way ANOVA followed by Tukey's test. Data are presented as the mean ± *SEM*. *$p < .05$, n.s.: nonsignificant. (f) Success rate (left), number of successful trials (center), and number of total trials (right) in early (Days 1–4), late (Days 9–12), and extended (Days 15–18) stages. Eight WT mice (red) and seven PLP-tg mice (blue) were used. Success rate: WT versus PLP-tg, $F_{1,39} = 24.6$, $p = .83$ (early), $p = .0012$ (late), $p = .047$ (extended); WT, $F_{2,39} = 35.5$, $p = 1.4 \times 10^{-6}$ (early vs. late), $p = 1.0$ (late vs. extended); PLP-tg, $F_{2,39} = 35.5$, $p = .044$ (early vs. late), $p = .73$ (late vs. extended), two-way ANOVA followed by Tukey's test. Success number: WT versus PLP-tg, $F_{1,39} = 17.2$, $p = .86$ (early), $p = .0022$ (late), $p = .42$ (extended); WT, $F_{2,39} = 18.8$, $p = 2.5 \times 10^{-4}$ (early vs. late), $p = 1.0$ (late vs. extended); PLP-tg, $F_{2,39} = 18.8$, $p = .58$ (early vs. late), $p = .37$ (late vs. extended), two-way ANOVA followed by Tukey's test. Total trial number: WT versus PLP-tg, $F_{1,39} = 2.74$, $p = .84$ (early), $p = .56$ (late), $p = 1.0$ (extended); WT, $F_{2,39} = 6.60$, $p = .25$ (early vs. late), $p = 1.0$ (late vs. extended); PLP-tg, $F_{2,39} = 6.60$, $p = .60$ (early vs. late), $p = .77$ (late vs. extended), two-way ANOVA followed by Tukey's test. Data are presented as the mean ± *SEM*. *$p < .05$, **$p < .01$, ***$p < .001$, n.s.: nonsignificant

Antidromic spikes were defined according to a previous report (Ciocchi, Passecker, Malagon-Vina, Mikus, & Klausberger, 2015), with slight modification (low spike jitter [<0.3 ms] and high fidelity [>50%] of light-induced spikes). One hundred and forty-one antidromic spikes from eight WT mice and 130 antidromic spikes from seven PLP-tg mice were analyzed. To estimate the temporal dispersion of antidromic spike latency, we calculated the SD and coefficient of variation using antidromic spikes that were detected simultaneously from more than two different channels in an experimental recording (20 × 20 ms pulses of a 470 nm LED stimulation at 1 Hz; WT, 136 antidromic spikes from 18 recordings; PLP-tg, 122 antidromic spikes from 19 recordings). Cortical spikes were analyzed from 99 units from seven WT mice and 112 units from six PLP-tg mice for optogenetic stimulation of the thalamocortical axons, and 95 units from six WT mice and 91 units from seven PLP-tg mice for optogenetic stimulation of the thalamus.

For the experiment on optogenetic stimulation of thalamic axons in M1 during motor learning, a fiber-optic cable was surgically implanted and secured over the left M1 in 5 WT mice or 16 PLP-tg mice, with the lever-pull task being commenced a week after the implantation. Blue light stimulation was provided by the same 470 nm LED in trains of 20 × 20 ms pulses delivered at 10 Hz. As a control, 5 WT mice or 10 PLP-tg mice injected with AAV2/1-Syn-GFP (1.18×10^{13} vector genomes/ml, UPenn Vector Core) received identical light stimulation during the lever-pull task. After 12 day training with the optogenetic stimulation, 10 of 16 PLP-tg mice with ChR2 expression further performed the task on days 13 and 14, without the optogenetic stimulation. The success rate in either early or late sessions was not different between PLP-tg mice and PLP-tg mice with GFP and the light stimulation ($F_{1,54}$ = 1.27, p = .95 [early], p = .72 [late], two-way ANOVA followed by Tukey's test). For the experiment on optogenetic stimulation of thalamic neurons during motor learning, a fiber-optic cable was implanted into the left motor thalamus in five PLP-tg mice. As a control, five PLP-tg mice injected with AAV2/1-Syn-GFP were used.

2.8 | Semi-quantitative RT-PCR

For analysis of mRNA expression, brains were removed from mice immediately after the final training session (Day 12), and cortical tissue from left and right coronal slices including M1 (1.5–0 mm from the bregma) was collected with a 1.0 mm diameter biopsy needle and frozen. RNA was extracted from the cortical tissue using TRIzol reagent (Invitrogen, Carlsbad, CA). Total RNA (2 μg) was reverse-transcribed with Superscript II and oligo-dT, and PCR was performed on a Roche Lightcycler (Roche, Minneapolis, MN) with FastStart DNA Master SYBR Green 1 PCR reaction mix. Relative expression levels in samples from the left and right hemispheres were quantified as previously described (Lee, Cohen, Tendi, Farrer, GH DEV, Becker KG, & Fields RD., 2004). Primer sequences were as follows: a housekeeping gene, glyceraldehyde phosphate dehydrogenase (GAPDH), 5-AAT GCATCCTGCACCACCAAC-3', 5'-TGGATGCAGGGATGATGTTCTG-3'; MBP, 5'-CGATTGGGTGTCACTCTGAAA-3', 5'-CCCAGCAGAGAAT GAACACAA-3'. For each tissue sample, the MBP mRNA expression level was normalized to that of GAPDH mRNA. For Figure 2d, 14 WT mice (six with and eight without training) and 15 PLP-tg mice (six with and nine without training) were used.

2.9 | Immunohistochemistry

After cardiac perfusion and overnight fixation with 4% paraformaldehyde in phosphate buffer (PB, pH 7.4), fixed brains were equilibrated in 30% sucrose solution in PB and cut into 20 μm-thick sections with a microtome (Leica Microsystems, Wetzlar, Germany). Sections were incubated overnight with anti-PV antibody (rabbit, Abcam ab 11,427; 1:1,000) in 10% normal goat serum/phosphate buffered saline with 0.3% Triton-X (pH 7.4) at 4°C, followed by 1 hr incubation with secondary antibody (Alexa Fluor 488 or 594 conjugated donkey anti-rabbit, Invitrogen). For 5-ethynyl-2′-deoxyuridine (EdU) labeling experiment, EdU was intraperitoneally administered (25 mg/kg) (Chehrehasa, Meedeniya, Dwyer, Abrahamsen, & Mackay-Sim, 2009) for 10 days before motor learning. Brain samples were removed from mice immediately after the final training session (Day 12). Fixed brain sections (20 μm) were incubated with anti-adenomatous polyposis coli (clone CC1) antibody (mouse, Calbiochem OP80; 1:500) followed by detection of EdU using the Alexa Fluor 555 Click-iT detection kit (Invitrogen). EdU and CC1 stained signals in the both motor cortex and corpse callosum were taken on an LSM 700 microscope (Zeiss) with a ×10 water-immersion objective (EC Plan-Neofluor, 0.3 NA; Zeiss) and then counted (motor cortex; 12 fields in four WT mice and 12 fields from four PLP-tg, subcortical white matter; nine fields in four WT mice and nine fields from four PLP-tg mice).

2.10 | Statistics

All data are presented as the mean ± *SEM*. Unpaired, paired, and one-sample *t* tests, Wilcoxon rank sum tests, ANOVA followed by Tukey's post hoc test and Pearson's correlation tests were used to test for statistical significance. The variances within each group of data were estimated. For Ca^{2+} imaging and electrophysiology data, the D'Agostino and Pearson normality test was first performed. Then, parametric or nonparametric tests were used to test for significance, depending on the data distribution.

3 | RESULTS

3.1 | PLP-tg mice show impairments of learning in a lever-pull task

We examined whether 2-month-old PLP-tg mice show impaired learning of a motor task: a self-initiated lever-pull task using the right forelimb (Hira et al., 2013; Masamizu et al., 2014) (Figure 1a). In this task, mice had to pull the lever and hold it there for 600 ms to receive a drop of water. Mice performed this task for 60 min per session (one session per day) during 12 sessions. First, we compared the time course of the 60 min-averaged task performance between wild-type

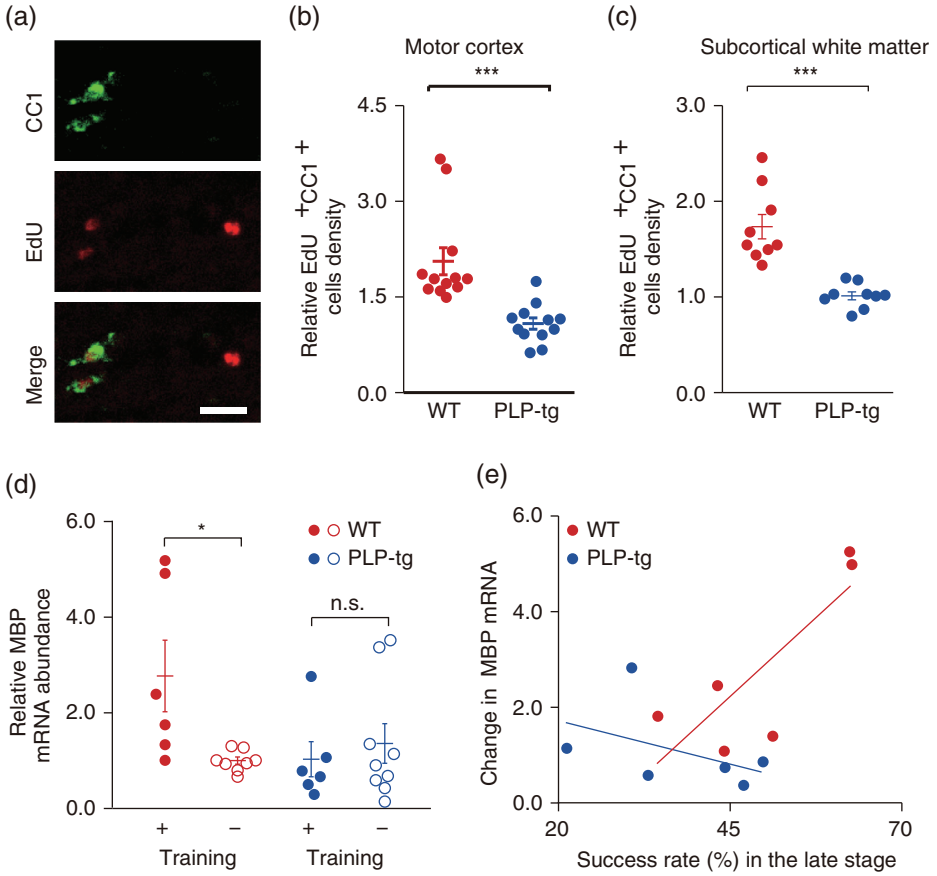

FIGURE 2 Changes in myelination during learning of a lever-pull task. (a) Typical images of EdU$^+$ CC1$^+$ cells in the subcortical white matter of M1 from WT mice. Scale bar, 20 μm. (b) Scatter plots of the ratio of EdU$^+$ CC1$^+$ cells density in the left gray matter of M1 to that in right gray matter of M1 ($p = 1.2 \times 10^{-4}$, n = 12 fields from four WT mice, n = 12 fields from four PLP-tg mice, Wilcoxon rank sum test). Data are presented as the mean ± *SEM*. ***$p < .001$. (c) Scatter plots of the ratio of EdU$^+$ CC1$^+$ cells density in the left subcortical white matter of M1 to that in right subcortical white matter of M1 ($p = 4.1 \times 10^{-5}$, n = nine fields from four WT mice, n = nine fields from four PLP-tg mice, Wilcoxon rank sum test). Data are presented as the mean ± *SEM*. ***$p < .001$. (d) The ratio of myelin basic protein (MBP) mRNA expression in left M1 to that in right M1 in trained and untrained WT and PLP-tg mice; $F_{3,25} = 3.29$, $p = .042$ (WT, training+ [$n = 6$] versus training− [$n = 8$]), $p = .95$ (PLP-tg, training+ [$n = 6$] versus training− [$n = 9$]), one-way ANOVA followed by Tukey's test. Data are presented as the mean ± *SEM*. *$p < .05$, n.s.: nonsignificant. (e) Changes in the MBP mRNA ratio against the success rate in the late training stage (WT: $n = 6$, $p = .049$, $r = 0.813$; PLP-tg: $n = 6$, $p = .37$, $r = -0.451$, Pearson's correlation test)

(WT) and PLP-tg mice. In the early training stage (Days 1–4), there was no difference between WT littermates and PLP-tg mice in either the success rate or the number of successful lever pulls (Figure 1b,c). In addition, the total number of lever-pull trials did not differ (Figure 1b,c). Thus, PLP-tg mice had the ability to move the forelimb, and recognized the association between the action (the lever-pull movement) and outcome (water reward). This is consistent with the lack of deficits exhibited by 2-month-old PLP-tg mice in other motor tests (wire hang, grip strength, and rotarod tests) (Tanaka et al., 2009). After sessions 1–4, the success rate of lever-pull trials continued to increase in both strains of mice (Figure 1b). However, in the late training stage (Days 9–12), the success rate and success number were lower in PLP-tg mice than in WT mice, although the total number of lever-pull trials was not different between WT and PLP-tg mice (Figure 1b,c). Even when we used the behavioral data during the initial 10 min of the session, when the mice were thought to be more highly motivated than during the following 50 min period, the success rate and success number in the late stage were lower in PLP-tg mice than in WT mice (Figure 1d). This indicates that although the motivation to receive the reward was not apparently different between WT and PLP-tg mice, the late-stage improvement in motor performance was impaired in PLP-tg mice.

It is possible that this impairment could be caused by enhanced anxiety (Tanaka et al., 2009); when the experiment was repeated with mice that had been habituated to the chamber for 1 week prior to the start of training, the difference in the success number in the late stage disappeared, but the difference in the success rate remained (Figure 1e). In the early sessions, the success rate or the number of successful trials did not differ (Figure 1e). Even when the training period was extended, the success rate in PLP-tg mice did not reach the level of that achieved by WT mice (Figure 1f). Furthermore, the number of successful or total lever pulls was not different between these two groups (Figure 1f). These results indicate that the low success rate in the late training stage in PLP-tg mice was not caused by

high anxiety under the task condition, and neither was it a direct result of their previously characterized abnormal behaviors.

Although the 60 min or initial 10 min-averaged task performance in the early sessions was not different between WT and PLP-tg mice (Figure 1b–d), changes in the performance within a session could still be different. If the memory for the task acquired in a session was maintained, the success rate should be high at the beginning of the next session (Costa, Cohen, & Nicolelis, 2004; Yin et al., 2009) and gradually decrease within the session as the water consumption increased. We divided the 60 min period into two 30 min periods, and compared the success rate between the initial 30 min period and the last 30 min periods. In WT mice, from session 4, the initial 30 min period showed a higher success rate than the last 30 min period (Supporting Information Figure S1). By contrast, in PLP-tg mice, the success rate of the initial 30 min was higher than that of the last 30 min period after session 7 (Supporting Information Figure S2). This result suggests that PLP-tg mice were relatively slow in retaining the motor memory from an earlier session in comparison with the WT mice.

In the following experiments, we used the success rate (60 min-averaged) as a robust behavioral indicator for the degree of motor learning, and examined what abnormal cellular functioning in the brain was associated with the low success rate in PLP-tg mice.

3.2 | Increase in myelin-related mRNA correlates with improvement of the task performance in WT mice

To determine whether lever-pull learning is related with the increase in myelination in gray and white matter of the left M1, as observed in other motor learning tasks (McKenzie et al., 2014; Sampaio-Baptista et al., 2013; Xiao et al., 2016), we first examined production of new myelinating oligodendrocytes associated with lever-pull learning in the gray and white matter of the left and right M1using immunohistochemistry. PLP-tg mice showed a lower ratio of the number of density (cells per mm^2) of EdU^+ $CC1^+$ cells in both left gray and white matter of M1 relative to right gray and white matter of M1 compared with those in WT (Figure 2a–c). This is consistent with the deficit of activity-dependent myelination in PLP-tg mice. Next, we measured the expression level of myelin basic protein (MBP) mRNA in trained and untrained WT mice because the thickness of myelin is mediated by MBP and correlates with MBP gene expression (Martini & Schachner, 1997; Shine, Readhead, Popko, Hood, & Sidman, 1992). Trained WT mice showed a higher ratio of MBP mRNA in the left M1 relative to the right M1 in comparison with untrained WT mice, whereas the ratio did not differ between trained and untrained PLP-tg mice (Figure 2d). The change in MBP mRNA positively correlated with the late training stage success rate in WT mice (p = .049, r = 0.813; Figure 2e), whereas in PLP-tg mice, there was not a significant association between the change in MBP mRNA and the late training stage success rate (p = .37, r = −0.451; Figure 2e). These results suggest that the increase in new myelinating oligodendrocytes (EdU^+ $CC1^+$) production and MBP mRNA expression were critical for the normal motor learning which was impaired in PLP-tg mice.

3.3 | Abnormalities of spontaneous cortical activity and task-related activity in PLP-tg mice

We examined how the deficits in the regulation of myelination in PLP-tg mice impaired the neural activity required for motor learning. We tested two simple possibilities in M1 neurons: whether PLP-tg mice showed lower task-related activity than WT mice, which would directly impair the motor execution, and whether PLP-tg mice showed higher spontaneous activity than WT mice, which would decrease the signal-to-noise ratio in the learning-relevant circuits. First, in the early and late training sessions, we conducted two-photon imaging of layer 2/3 (L2/3) neurons in M1, which expressed GCaMP3 (Tian et al., 2009) (Figure 3a). Two to 3 weeks before the training started, we injected an adeno-associated virus (AAV) carrying the GCaMP3 gene into the left M1. We used synapsin I promotor so that GCaMP3 was mainly expressed in excitatory neurons (Masamizu et al., 2014; O'Connor, Peron, Huber, & Svoboda, 2010). Many GCaMP3-expressing neurons showed Ca^{2+} transients, both during the lever-pull movement and outside of the movement (Figure 3b). We divided each imaging session into three periods: a task-related period that started 1.2 s before and ended 1.6 s after the start point of successful lever pulling behavior, a spontaneous period that was outside of the period from 1.2 s before and ending 1.6 s after the start point of any lever pull, and a third "other" period, which included failed trials (Figure 3c). We then calculated the frequency and amplitude of Ca^{2+} transients in the task-related and spontaneous periods (Figure 3c; see more details in Materials and Methods). There was no difference between WT and PLP-tg mice in the frequency of task-related Ca^{2+} transients in either the early or the late training stage. By contrast, in both training stages, the amplitude of task-related Ca^{2+} transients was smaller in PLP-tg mice than in WT mice (Figure 3d,e and Table 1; see Materials and Methods). The frequency of spontaneous Ca^{2+} transients was significantly larger in PLP-tg mice than in WT mice in both training stages, while the amplitude was significantly smaller (Figure 3d,e and Table 1). When the task-related period was set to be longer or shorter than that stated above, the results were similar (Table 1). Thus, in both early and late sessions, PLP-tg mice showed lower task-related Ca^{2+} transients, and a higher frequency and smaller amplitude of spontaneous Ca^{2+} transients than WT mice.

We confirmed the increased spontaneous firing in awake PLP-tg mice without any training by performing multi-unit recordings from L2/3 and L5 in M1 (Figure 4a–c). When excitatory synaptic transmission was blocked, spontaneous firing in PLP-tg mice reduced (Figure 4d,e). This was similar to the result obtained in a mouse model of Alzheimer's disease (Busche et al., 2008). Anesthesia substantially reduced the frequency of spontaneous firing and abolished the difference between WT and PLP-tg mice (Figure 4f,g). The frequency of spontaneous Ca^{2+} transients on each day of training was inversely correlated with the change in success rate from that day to the next, with this being the case in any WT and PLP-tg mice, which was statistically significant (Figure 3f). This implies that day-by-day fluctuations in spontaneous activity could affect the motor learning performance at each day.

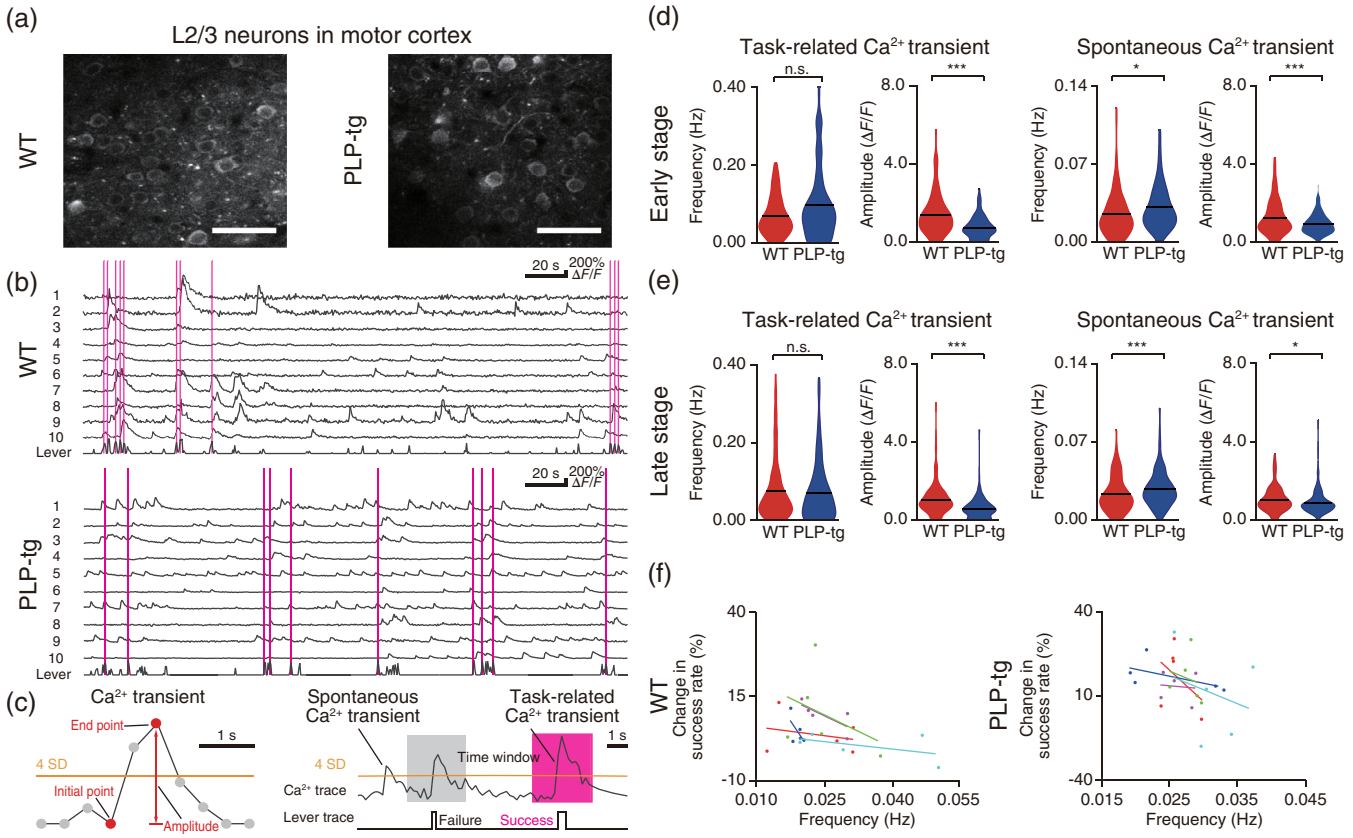

FIGURE 3 Task-related and spontaneous neuronal activity during learning. (a) Typical images of L2/3 M1 neurons expressing GCaMP3 in WT (left) and PLP-tg (right) mice. Scale bar, 50 μm. (b) Representative Ca^{2+} traces of 10 neurons and the corresponding lever trajectory (bottom trace in each panel) on Day 1 in WT (top) and PLP-tg (bottom) mice. The magenta vertical lines indicate successful lever pulls. (c) Schematics of task-related Ca^{2+} transients and spontaneous Ca^{2+} transients (see more details in Methods). (d, e) Violin plots (black lines, mean) of the frequency and amplitude of task-related and spontaneous Ca^{2+} transients in the early stage (d, task-related: frequency, $p = .051$, $n = 128$ from five mice [WT] and $n = 158$ from five mice [PLP-tg], Wilcoxon rank sum test; amplitude, $p = 5.2 \times 10^{-10}$, unpaired t test; spontaneous: frequency, $p = .010$, Wilcoxon rank sum test; amplitude, $p = 7.0 \times 10^{-4}$, unpaired t test) and late stage (e, task-related: frequency, $p = .38$, $n = 187$ from five mice [WT] and $n = 199$ from five mice [PLP-tg], Wilcoxon rank sum test; amplitude, $p = 2.6 \times 10^{-11}$, unpaired t test; spontaneous: frequency, $p = 4.8 \times 10^{-4}$, Wilcoxon rank sum test; amplitude, $p = .020$, unpaired t test). *$p < .05$, ***$p < .001$, n.s.: nonsignificant. (f) Correlation between the median frequency of spontaneous Ca^{2+} transients on each day and the change in the lever-pull success rate from that day to the next. Data are from five WT and five PLP-tg mice on Days 1, 3, 5, 7, and 9. Data from individual mice are plotted in different colors. For five WT mice, $r = -0.498 \pm 0.082$, $p = .0037$, one-sample t test. For five PLP-tg mice, $r = -0.309 \pm 0.086$, $p = .023$, one-sample t test

3.4 | PLP-tg mice had no defects in spontaneous activity of inhibitory neurons

The increased spontaneous activity in mouse models of Alzheimer's disease (Busche et al., 2008) and fragile X syndrome (Goncalves et al., 2013) is related to defects in inhibition, and is detected even in the anesthetized state. Thus, we tested whether the origin of the increased spontaneous activity in PLP-tg mice was related to the abnormality in inhibitory neurons. We performed two-photon Ca^{2+} imaging of L2/3 PV-positive neurons on Day 1 of training (Figure 5a, b). We crossbred PLP-tg with PV-Cre mice (Tanahira et al., 2009), and injected an AAV coding GCaMP6f (Chen et al., 2013), which expressed in a Cre-dependent manner. The frequency and amplitude of the spontaneous Ca^{2+} transients of these neurons were not different between WT and PLP-tg mice (Figure 5c and Table 1). The frequency and amplitude of task-related Ca^{2+} transients also showed no differences between these two groups (Figure 5c and Table 1). These results indicate that the learning impairment in PLP-tg mice is not mainly caused by a defect in the activity of inhibitory neurons.

In the following experiments, we tested whether changes in the axonal conduction of myelinated long-range axons in PLP-tg mice were associated with the abnormal M1 neuronal activity and low success rate.

3.5 | Temporal dispersion of axonal conduction in PLP-tg mice

First, we tested whether the axonal conduction of myelinated long-range axons projecting to M1 varied in PLP-tg mice. Thalamic neurons, including motor thalamic neurons, strongly innervate M1, and regulate cortical activity (Bosch-Bouju, Hyland, & Parr-Brownlie, 2013; Hooks et al., 2013); moreover, regulation of CV in myelinated thalamocortical axons during development ensures that inputs arrive synchronously (Salami,

TABLE 1 Results of Ca^{2+} image analysis using long and short task-related periods

Task-related Ca^{2+} transient (early stage)						
Time window	**1**			**2**		
Mouse, *p* value	WT	PLP-tg	*p* value	WT	PLP-tg	*p* value
Frequency (Hz)	0.075 ± 0.005	0.099 ± 0.008	.49	0.069 ± 0.004	0.097 ± 0.008	.056
Amplitude (Δ*F*/*F*)	1.503 ± 0.091	0.866 ± 0.044	3.0×10^{-9}	1.540 ± 0.091	0.886 ± 0.043	9.6×10^{-10}
Spontaneous Ca^{2+} transient (early stage)						
Time window	1			2		
Mouse, *p* value	WT	PLP-tg	*p* value	WT	PLP-tg	*p* value
Frequency (Hz)	0.027 ± 0.002	0.031 ± 0.002	.049	0.026 ± 0.002	0.030 ± 0.002	.034
Amplitude (Δ*F*/*F*)	1.338 ± 0.074	0.960 ± 0.041	1.3×10^{-5}	1.304 ± 0.079	0.951 ± 0.040	9.7×10^{-5}
Task-related Ca^{2+} transient (late stage)						
Time window	1			2		
Mouse, *p* value	WT	PLP-tg	*p* value	WT	PLP-tg	*p* value
Frequency (Hz)	0.085 ± 0.008	0.070 ± 0.006	.075	0.075 ± 0.006	0.069 ± 0.006	.18
Amplitude (Δ*F*/*F*)	1.107 ± 0.050	0.718 ± 0.043	1.0×10^{-10}	1.120 ± 0.056	0.703 ± 0.038	2.3×10^{-9}
Spontaneous Ca^{2+} transient (late stage)						
Time window	1			2		
Mouse, *p* value	WT	PLP-tg	*p* value	WT	PLP-tg	*p* value
Frequency (Hz)	0.025 ± 0.001	0.029 ± 0.001	7.1×10^{-3}	0.022 ± 0.001	0.027 ± 0.001	1.9×10^{-4}
Amplitude (Δ*F*/*F*)	1.096 ± 0.045	0.887 ± 0.040	5.4×10^{-4}	1.080 ± 0.044	0.885 ± 0.040	1.4×10^{-3}
Task-related Ca^{2+} transient (PV neurons)						
Time window	1			2		
Mouse, *p* value	WT	PLP-tg	*p* value	WT	PLP-tg	*p* value
Frequency (Hz)	0.409 ± 0.016	0.372 ± 0.014	.054	0.362 ± 0.012	0.341 ± 0.012	.11
Amplitude (Δ*F*/*F*)	2.880 ± 0.235	2.940 ± 0.188	.84	2.825 ± 0.221	2.945 ± 0.195	.68
Spontaneous Ca^{2+} transient (PV neurons)						
Time window	1			2		
Mouse, *p* value	WT	PLP-tg	*p* value	WT	PLP-tg	*p* value
Frequency (Hz)	0.036 ± 0.002	0.044 ± 0.002	.054	0.033 ± 0.002	0.041 ± 0.001	.071
Amplitude (Δ*F*/*F*)	1.790 ± 0.109	1.912 ± 0.109	.43	1.728 ± 0.106	1.859 ± 0.107	.39

To validate the statistical significance of Figure 3d,e and Figure 5c, two different time windows were used to redefine the task-related Ca^{2+} transients and spontaneous Ca^{2+} transients. Time window 1 started 0.8 s before and ended 1.2 s after the start of successful lever-pull trials (short). Time window 2 started 1.2 s before and ended 2 s after the start of successful lever-pull trials (long). All data are presented as the mean ± *SEM*. Unpaired *t* tests and Wilcoxon rank sum tests were used to test for statistical significance.

Itami, Tsumoto, & Kimura, 2003). Therefore, we measured the conduction time of antidromic spikes of thalamic axons projecting to M1 in PLP-tg mice. We injected an AAV carrying the channelrhodopsin-2 (ChR2) gene into the thalamus, including the motor thalamus (Figure 6a). We then recorded antidromically evoked spikes in the thalamus, while optogenetically stimulating the thalamic axons in M1 with blue light at 1 Hz (Figure 6a,b). In both WT and PLP-tg mice, spikes with very short jitter (~0.15 ms) and high fidelity (~80%) were evoked (Figure 6c,d). These parameters did not differ between WT and PLP-tg mice (Figure 6d). Thus, optogenetic activation reliably evoked antidromic spikes in the same thalamic neurons in both mice. In the antidromic spikes, the spike latency from the onset of the stimulation was longer in PLP-tg mice than in WT mice (Figure 6e). Furthermore, the temporal dispersion of the antidromic spike latency across different recording channels in the same animal was broader in PLP-tg mice than in WT mice (Figure 6f). These results demonstrate that in PLP-tg mice the axonal conduction in thalamocortical axons was not only reduced but also temporally spread.

3.6 | Stimulation of thalamic neurons evoked asynchronous cortical activity in PLP-tg mice

Second, we measured M1 activity responding to the optogenetic stimulation of the thalamic axons in M1 (Figure 7a). When these were stimulated at 1 Hz, spikes in L2/3 of M1 were evoked in similar

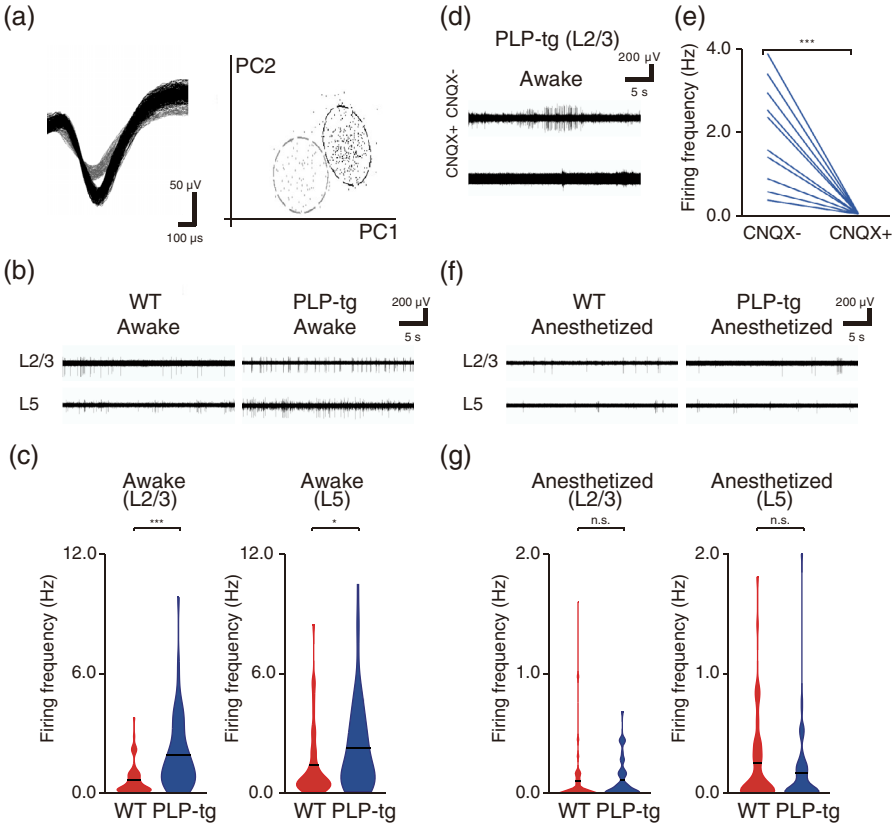

FIGURE 4 Properties of spontaneous firing in L2/3 and L5 neurons. (a) Representative traces from two putative independent units recorded on a single channel and their separation in first and second principle component space. (b) Typical extracellular recordings from L2/3 and L5 in awake WT (left) and PLP-tg (right) mice. (c) The spontaneous firing rates of L2/3 (left) and L5 (right) neurons during the awake state (L2/3: $p = 2.3 \times 10^{-10}$, n = 68 units from 10 WT mice, n = 56 units from 13 PLP-tg mice; L5: p = .049, n = 55 units from nine WT mice, n = 58 units from nine PLP-tg mice, Wilcoxon rank sum test). Violin plot shows mean (black lines) and distribution of the data. *p < .05, ***p < .001. (d) Typical traces from recordings in L2/3 neurons in awake PLP-tg mice before and after CNQX application. (e) Spontaneous firing rate before and after CNQX application in awake PLP-tg mice ($p = 6.6 \times 10^{-4}$, n = 10 units from four mice, paired t test). ***p < .001. (f) Typical extracellular recordings from L2/3 and L5 in anesthetized WT (left) and PLP-tg (right) mice. (g) The spontaneous firing rates of L2/3 (left) and L5 (right) neurons during anesthetized states (L2/3: p = .36, n = 63 units from 10 WT mice, n = 51 units from 12 PLP-tg mice; L5: p = .66, n = 55 units from nine WT mice, n = 58 units from nine PLP-tg mice, Wilcoxon rank sum test). Violin plot shows mean (black lines) and distribution of the data. n.s.: nonsignificant

patterns across stimuli (Figure 7a–c). The durations of evoked spike volleys, which were defined as the average durations between the first and last evoked spikes in individual stimuli, were no different between WT and PLP-tg mice (Figure 7d). This indicates that neither the timing to evoke the axonal firing after the optogenetic stimulation, nor the process from the thalamocortical synaptic transmission to the firing of cortical neurons was different between the WT and PLP-tg mice.

Third, we measured the M1 activity responding to the optogenetic stimulation of the somata of the thalamic neurons (Figure 7a). In this case, the duration of the spike volleys evoked in M1 was significantly longer in PLP-tg mice than in WT mice (Figure 7a–c,e). This indicates that in PLP-tg mice the long-range thalamocortical axons with a wide range of axonal conduction substantially spread the timings of presynaptic neurotransmitter release and postsynaptic firing in M1. In addition, the number of spikes evoked by optogenetic stimulation of the thalamus was significantly larger in PLP-tg mice than in WT mice (Figure 7f). This implies that the prolonged postsynaptic spike volleys could be a factor increasing the spontaneous activity.

3.7 | Synchronous stimulation of thalamic afferents rescues the learning performance in PLP-tg mice

If asynchronous activity in thalamocortical axons impaired the late-stage success rate in PLP-tg mice, artificial synchronous activity in thalamocortical axons during the lever-pull movement would raise the decreased task-related activity, and could restore the success rate. The electrical stimulation of thalamocortical axons at 10 Hz augments motor cortical activity (Castro-Alamancos, 2013; Miall et al., 1998). ChR2 stimulation of thalamocortical axons at 5 or 10 Hz enhances the recovery of somatosensory cortical circuit function and forepaw sensorimotor abilities after stroke (Tennant, Taylor, White, & Brown, 2017). In our experimental condition, 10 Hz stimulation of thalamocortical axons reliably induced the cortical response in WT

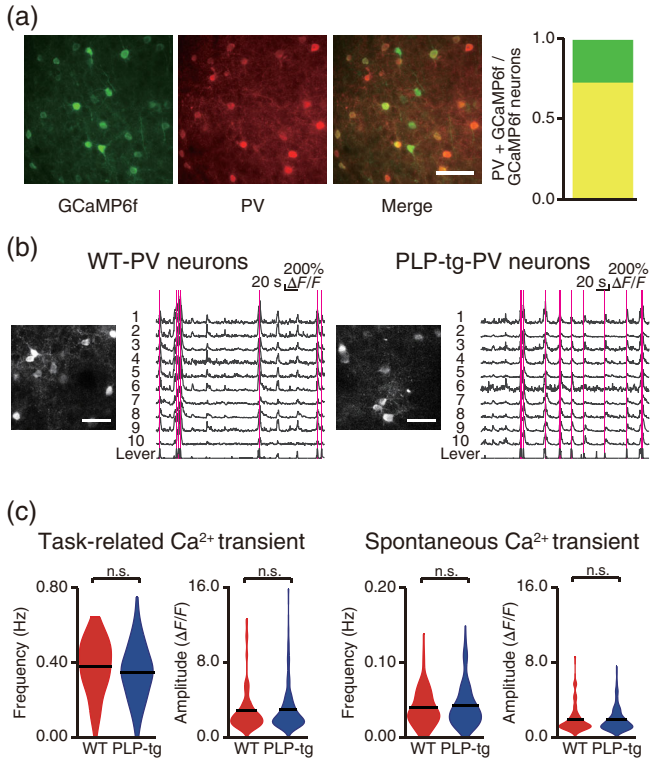

FIGURE 5 PLP-tg mice did not have apparent defects in the function of inhibitory neurons. (a) GCaMP6f expression and PV immunostaining from a PV-Cre mouse that was injected with rAAV2/1-CAG-flex-GCaMP6f. Proportion of PV-positive neurons (yellow) out of all GCaMP6f-expressing neurons (142 PV-positive neurons and 194 GCaMP6f-expressing neurons in four slices from two mice). Scale bar, 50 μm. (b) Representative two-photon images, Ca^{2+} traces, and the corresponding lever trajectory (bottom trace in each plot) from a WT/PV-Cre mouse (left) and PLP-tg/PV-Cre mouse (right) recorded during the task on Day 1. The magenta vertical lines indicate successful lever pulls. Scale bar, 50 μm. (c) The frequency and amplitude of task-related and spontaneous Ca^{2+} transients in PV neurons on Day 1 (n = 115 from five fields in four WT/PV-Cre mice, n = 145 from nine fields in five PLP-tg/PV-Cre mice, task-related: frequency, p = .051, Wilcoxon rank sum test; amplitude, p = .63, unpaired t test; spontaneous: frequency, p = .72, Wilcoxon rank sum test; amplitude, p = .86, unpaired t test). Violin plot shows the mean (black lines) and distribution of the data. n.s.: nonsignificant

mice (the average number of M1 unit responses to the stimulation was 1.93 ± 0.08, n = 31 units from two mice). Therefore, for the mice with ChR2 or GFP expression in thalamic neurons, repetitive optogenetic stimulation at 10 Hz (Castro-Alamancos, 2013; Miall et al., 1998) was applied to thalamocortical axons in M1 immediately after the onset of each lever pull in each training session (Figure 8a). In the early training stage, the success rate was not different between ChR2-expressing and GFP-expressing PLP-tg mice. However, in the late stage, ChR2-expressing PLP-tg mice showed slightly but significantly higher lever-pull success rate than GFP-expressing mice (Figure 8b,c). In addition, the success rate in both early and late stage was not different between ChR2-expressing and GFP-expressing WT mice that already received synchronized inputs from thalamus before thalamocortical axons stimulation (Figure 8d,e). Thus, the formation of synchronous activity in thalamocortical axons during learning-relevant movements was able to partially restore the success rate of PLP-tg mice, not WT mice, in the late training stage, indicating that this contribution was only present in myelin deficient mice.

Next, to assess whether activation of thalamic activity also contributes to behavior improvement, we trained the PLP-tg mice having ChR2 or GFP expression in the thalamus with the stimulation of thalamic cell bodies. In the early training stage, the success rate was not different between ChR2-expressing and GFP-expressing mice. However, in the late stage, ChR2-expressing mice showed significantly higher success rates than GFP-expressing mice (Figure 8f,g). Optogenetic stimulation of thalamic cell bodies with lever pulling might improve thalamic activity by compensating dispersed inputs from basal ganglia and cerebellum that are crucial for motor learning (Bosch-Bouju et al., 2013; Tanaka et al., 2018). Furthermore, in ChR2-expressing mice, from session 5 onward, the initial 30 min period showed a higher success rate than the last 30 min periods (Supporting Information Figure S3), in contrast, in GFP-expressing mice, the success rate of the initial 30 min was higher than that of the last 30 min period after session 9 (Supporting Information Figure S4). Therefore, the facilitation of thalamic activity during learning-relevant movements was also able to restore the success rate in PLP-tg mice.

Finally, we determined whether the optogenetic stimulation of thalamocortical axons was still helpful for the lever-pull movement after 12 day training in PLP-tg mice. A subset of the PLP-tg mice that had performed the task with the stimulation throughout training Days 1–12 performed the task without the stimulation on Days 13 and 14. The mean success rate over Days 11 and 12 was not different from that over Days 13 and 14 (Figure 8h). This result suggests that the synchronous input of thalamocortical axons was critical to form the M1 neuronal activity required for skill acquisition, and that after training this M1 activity might be induced without the assistance of the synchronous input of thalamocortical axons.

4 | DISCUSSION

This study demonstrates that impaired myelination increases axonal conduction variability in long-range axons, thereby leading to a greater spread in the timing of synaptic transmission and postsynaptic activity, and that this abnormality can be the origin of other abnormalities of the neural circuits, such as weak task-related activity and high basal activity. The weak task-related activity is presumably caused by a decrease in the coincident long-range synaptic inputs required for induction of strong burst firing in postsynaptic neurons (Figure 9). The abnormally high basal activity observed in PLP-tg mice may be caused by occasionally occurring synchronous events of temporally-spread synaptic transmission from many distant areas. These abnormalities would weaken the propagation of information and STDP within cortical networks (Moldakarimov, Bazhenov, & Sejnowski, 2015; Pajevic et al., 2014) and may deprive neurons of the ability to regulate activity-dependent myelination in respect to white matter plasticity

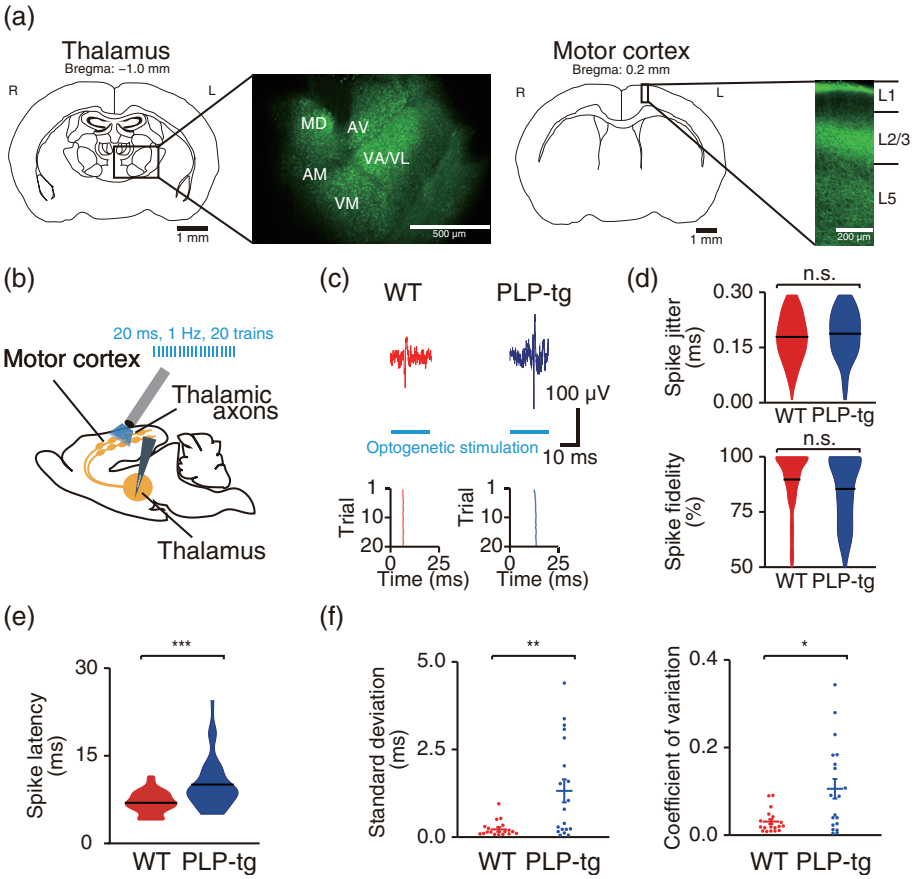

FIGURE 6 Temporal dispersion of axonal conduction in thalamocortical axons. (a) ChR2 expression in the thalamus and thalamocortical axons. Representative images of ChR2-EYFP expression in the thalamus (left) and motor cortex (right) after AAV2/1-Syn-ChR2 (H134R)-EYFP injection into the thalamus. (b) Experimental design of antidromic spike induction. (c) Top, representative examples of spikes detected in the thalamus in response to optogenetic stimulation of thalamic afferents in M1. Bottom, typical examples of raster plots. Each of 20 stimulation trials is plotted as a single row. (d) Violin plots (black lines, mean) of the spike jitter and spike fidelity of evoked spikes (spike jitter, $p = .20$; spike fidelity, $p = .059$, $n = 141$ antidromic spikes from eight anesthetized WT mice, $n = 130$ antidromic spikes from seven anesthetized PLP-tg mice, Wilcoxon rank sum test). n.s.: nonsignificant. (e) Violin plots (black lines, mean) of the latency of antidromic spikes evoked in response to optogenetic stimulation of thalamic afferents ($p = 2.6 \times 10^{-13}$, $n = 141$ antidromic spikes from eight anesthetized WT mice, $n = 130$ antidromic spikes from seven anesthetized PLP-tg mice, Wilcoxon rank sum test). ***$p < .001$. (f) Scatter plots of the temporal dispersion of antidromic spike latency (standard deviation, $p = .0065$; coefficient of variation, $p = .017$, $n = 18$ recordings in WT mice, $n = 19$ recordings in PLP-tg mice, Wilcoxon rank sum test). *$p < .05$, **$p < .01$

(Hines et al., 2015; Mensch et al., 2015; Wake et al., 2011; Wake et al., 2015). During development, myelination changes the CV of thalamocortical pathways to increase synchronicity of the cortical activity, which may facilitate cortical information processing (Kimura & Itami, 2009; Salami et al., 2003). It should be clarified in the future whether and to what extent the CVs of thalamocortical axons become increasingly synchronized, and their synapses or downstream synapses show STDP during learning processes.

Abnormally high basal activity in the cerebral cortex is also a feature in Alzheimer's disease (Busche et al., 2008) and Fragile X syndrome (Goncalves et al., 2013) mouse models. PLP-tg mice at 2 months of age show behavioral abnormalities related to schizophrenia (Tanaka et al., 2009). Taken together, abnormally high basal activity may be a common phenotype in neurological and psychiatric disorders. Even in WT mice, the low basal activity on a given day tended to be correlated with the increase in the success rate on that day. In WT mice, the basal activity was lower than in PLP-tg mice and varied daily, and therefore this effect may not be distinguished over training sessions. In the mouse models of Alzheimer disease (Busche et al., 2008) and Fragile X syndrome (Goncalves et al., 2013), high basal activity was also detected in the anesthetized state, whereas the basal activity was similar between anesthetized WT and PLP-tg mice. In contrast to the former mouse models, PLP-tg mice did not show any apparent defect in inhibition. Thus, the underlying mechanism was probably different. If the abnormal basal activity generally precedes the behavioral deficits, it may be a preclinical phenotype.

The motor impairment in PLP-tg mice was not clearly detected in the early training stage. However, during the early training stage, the success rate of initial 30 min period was higher compared to that of the last 30 min period in PLP-tg mice than in WT mice. This suggests that the improvement in the task performance in an early session was

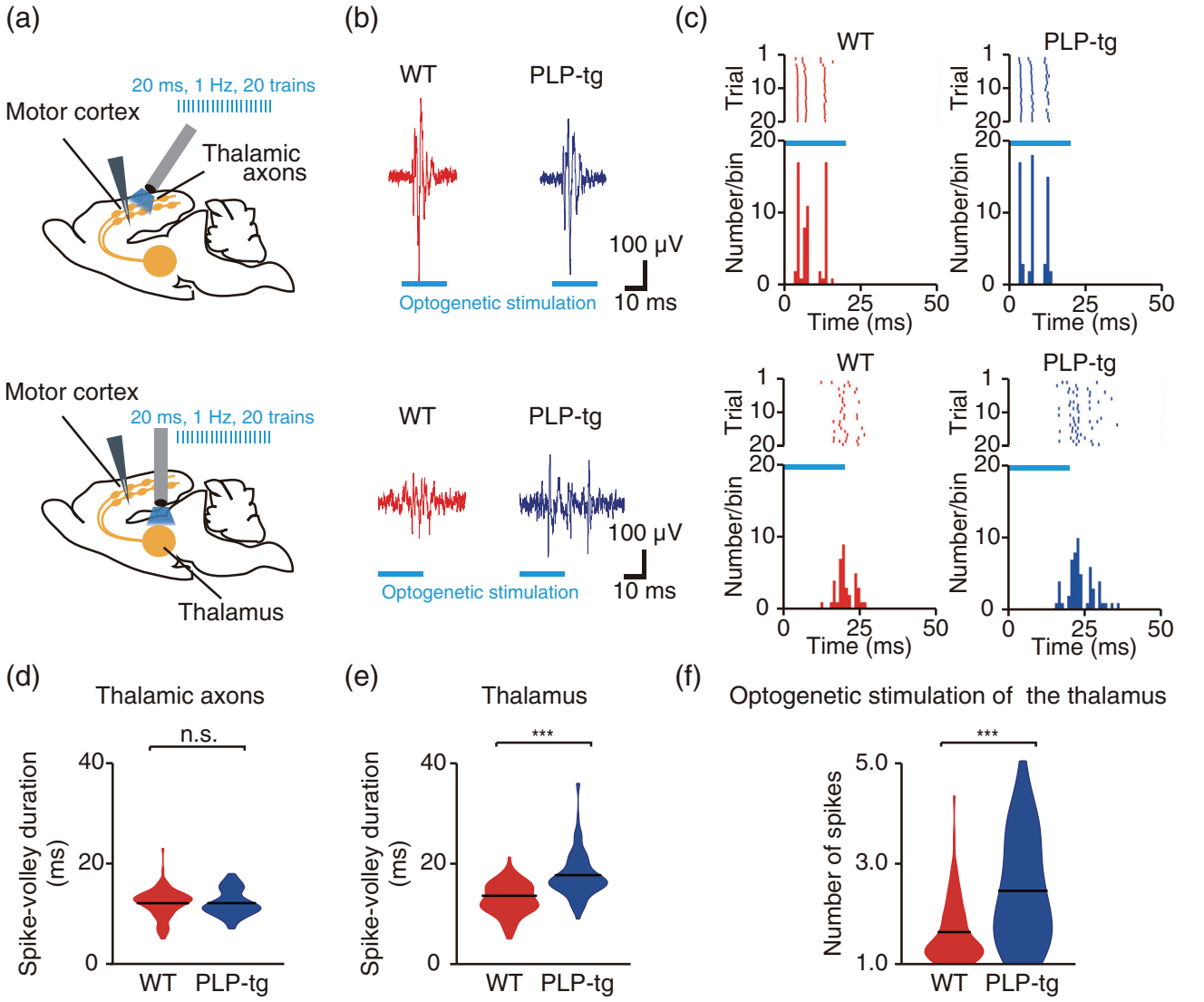

FIGURE 7 Temporal dispersion of M1 cortical responses to thalamic stimulation. (a) Experimental design of optogenetic stimulation of the thalamocortical axons in M1 (top) and thalamus (bottom). (b) Representative examples of spike volleys in L2/3 in response to optogenetic stimulation of the motor cortex (top) or thalamus (bottom). (c) Typical examples of raster plots (top, each representation of 20 stimulation trials is plotted as a single row) and corresponding peri-event time histograms (bottom). (d) Violin plots (black lines, mean) of the duration of spike volleys evoked in response to optogenetic stimulation of thalamic axons (p = .20, n = 99 units from seven anesthetized WT mice, n = 112 units from six anesthetized PLP-tg mice, Wilcoxon rank sum test). n.s.: nonsignificant. (e) Violin plots (black lines, mean) of the duration of spike volleys evoked in response to optogenetic stimulation of thalamic somata ($p = 5.2 \times 10^{-12}$, n = 95 units from six anesthetized WT mice, n = 91 units from seven anesthetized PLP-tg mice, Wilcoxon rank sum test). ***p < .001. (f) Violin plots (black lines, mean) of the number of spikes evoked by optogenetic stimulation of the thalamus ($p = 2.9 \times 10^{-5}$, n = 95 units from six anesthetized WT mice, n = 91 units from seven anesthetized PLP-tg mice, unpaired t test). ***p < .001

barely retained by the time of the next session. Motor learning can be divided into two stages: associative learning in the early stage and skill learning in the late stage (Balleine & O'Doherty, 2010; Doyon & Benali, 2005; Makino, Hwang, Hedrick, & Komiyama, 2016). In the late training stage, which may correspond to the skill learning stage, the coordinated movement of forelimb and other body parts may be acquired by long-range signal transmission including sensory inputs from the periphery and cerebellum to the cerebral cortex through the thalamus (Bosch-Bouju et al., 2013; Shadmehr & Krakauer, 2008). In such a case, the synchronous input of myelinated long-range axons connecting distant areas, and information processes with a high signal-to-noise ratio, may be important (Gibson et al., 2014; McKenzie et al., 2014; Xiao et al., 2016). In contrast to our results, the effect of impaired myelin regulation was detected from the beginning of motor training in other studies (McKenzie et al., 2014; Xiao et al., 2016). These assessed motor learning ability using a running wheel with irregularly spaced rungs, in which the mice had to coordinate many parts of the body to avoid missing their step, even in the first session. This task may have a much greater requirement for synchronous long-range axonal transmission than the task we used, and the effect of impaired myelination may be apparent and detectable from the first to the final session.

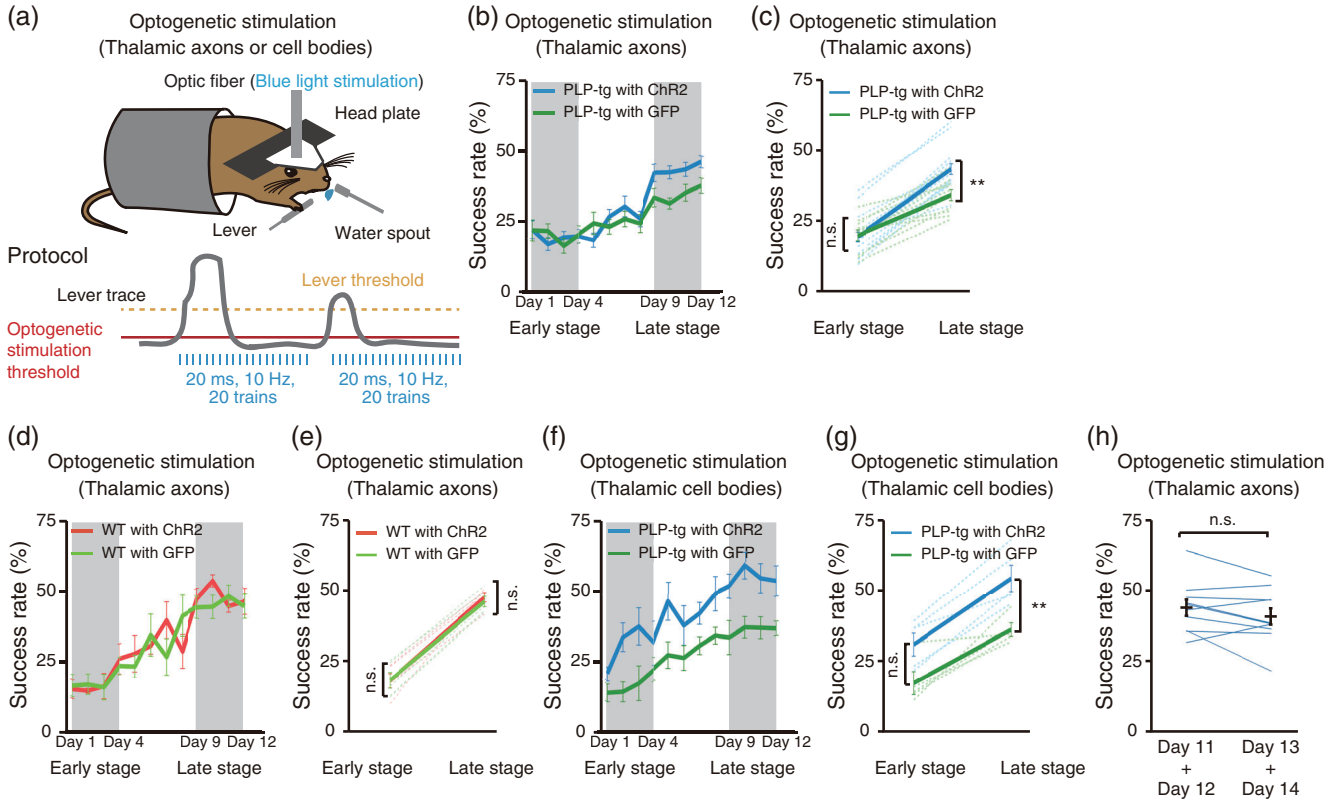

FIGURE 8 Effects of optogenetic stimulation of thalamic neurons on motor learning. (a) Schematic of the optogenetic stimulation-assisted lever-pull task. Repetitive optogenetic stimulation of thalamocortical axons or thalamic cell bodies was triggered when the lever position crossed a threshold. (b) Time course of the 60 min-averaged lever-pull success rate in PLP-tg mice with optogenetic stimulation of ChR2- (n = 16; light blue) or GFP- (n = 10; green) expressing thalamocortical axons. (c) Success rate in early (Days 1–4) and late (Days 9–12) training stages in PLP-tg mice with blue light illumination of ChR2- (light blue) or GFP- (green) expressing thalamocortical axons ($F_{1,48}$ = 4.73, p = 1.0 [early], p = 0.0097 [late], two-way ANOVA followed by Tukey's test). Data are presented as the mean ± *SEM*. **p < .01, n.s.: nonsignificant. (d) Time course of the 60 min-averaged lever-pull success rate in WT mice with optogenetic stimulation of ChR2- (n = 5; light red) or GFP- (n = 5; light green) expressing thalamocortical axons. (e) Success rate in early (Days 1–4) and late (Days 9–12) training stages in WT mice with ChR2- (light red) or GFP- (light green) expressing thalamocortical axons during optogenetic stimulation ($F_{1,16}$ = 0.09, p = 1.0 [early], p = .97 [late], two-way ANOVA followed by Tukey's test). Data are presented as the mean ± *SEM*. n.s.: nonsignificant. (f) Time course of the 60 min-averaged lever-pull success rate in PLP-tg mice with optogenetic stimulation of ChR2- (n = 5; light blue) or GFP- (n = 5; green) expressing thalamic cell bodies. (g) Success rate in early (Days 1–4) and late (Days 9–12) training stages in PLP-tg mice with ChR2- (light blue) or GFP- (green) expressing thalamic cell bodies during optogenetic stimulation ($F_{1,16}$ = 20.63, p = .063 [early], p = .0098 [late], two-way ANOVA followed by Tukey's test). Data are presented as the mean ± *SEM*. **p < .01, n.s.: nonsignificant. (h) Success rates averaged over Days 11 and 12 (left) and over Days 13 and 14 (right) in ChR2-expressing PLP-tg mice with optogenetic stimulation during Days 1–12, but not Days 13 and 14 (p = .24, n = 10, paired t test). Black lines indicate the mean ± *SEM*. n.s.: nonsignificant

We demonstrated that motor learning could be restored by optogenetically stimulating a population of thalamocortical axons and thus overcoming asynchrony in long-range synaptic inputs. However, the extent of the rescue appeared partial because the late training stage success rate in this experiment (Figure 8c) was lower than that in the normal training schedule in WT mice (Figure 1c). The reason why the restoration was partial may be that other long-range axons such as the pyramidal tracts were involved in the motor learning. In addition, the duration of the optogenetic assistance was limited to the lever-pull movement, so the effect of the high frequency of basal activity remained in the late training stage. It is perhaps surprising that facilitating the synchronization of only one myelinated pathway was effective in restoring learning. This suggests that the synchronicity of the spike-time arrival in the thalamocortical pathway has a great influence on learning. In addition, activation of thalamic cell bodies also contributes to improvement of motor learning. Inputs from basal ganglia and cerebellum mediating motor thalamus are crucial for motor learning (Bosch-Bouju et al., 2013; Tanaka et al., 2018). Therefore, optogenetic stimulation of thalamic cell bodies with lever pulling might restore the success rate in PLP-tg mice by either or both of increase in thalamic activity itself and/or partial compensation of dispersed inputs from basal ganglia and cerebellum to motor nucleus of thalamus. Furthermore, a subset of PLP-tg mice (10 of 16 PLP-tg mice) with the optogenetic assistance during training Days 1–12 performed the task with a similar success rate without the stimulation on Days 13 and 14. One interpretation of this result might be that cortical neurons in the descending pathway of the thalamocortical inputs are able to maintain the partially rescued performance once it has

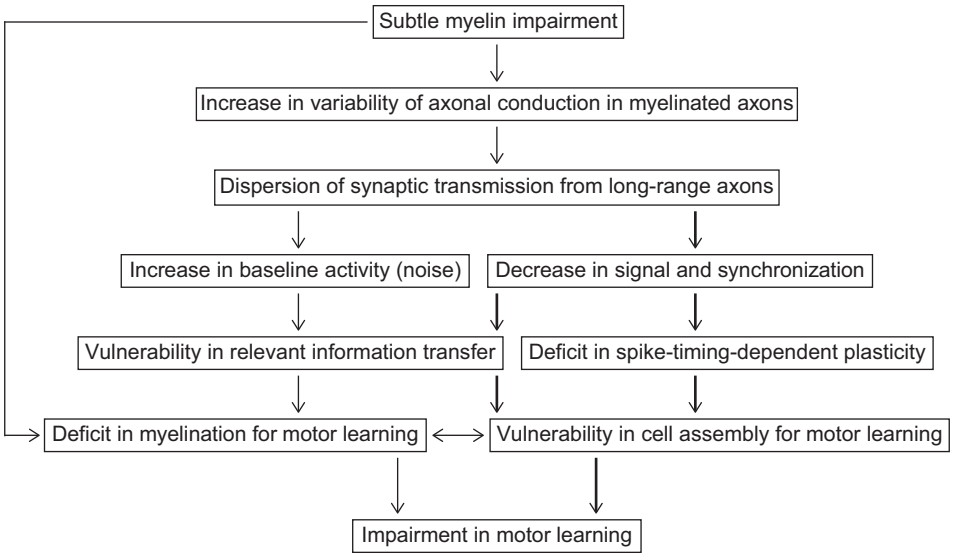

FIGURE 9 Proposed mechanisms by which subtle myelin dysregulation causes motor learning impairment. Optogenetic stimulation of thalamocortical axons was assumed to partially rescue the pathways indicated by thick arrows

formed. Another interpretation of this result might be that an antidromic activity in thalamo-cortical axons induced by optogenetic stimulation contributes to activity-dependent myelination that promotes synchrony of spike time arrival. In psychiatric diseases such as schizophrenia, subtle impairment of myelin regulation and thalamocortical dysrhythmia are observed (Hakak et al., 2001; Nave & Ehrenreich, 2014; Schulman et al., 2011). In the much larger human brain, myelin regulation of cortico-cortical long-range axons such as transcallosal cortical projections is also crucial (Nave, 2010), and is necessary for cognition and learning (Nave & Ehrenreich, 2014; Whitford, Ford, Mathalon, Kubicki, & Shenton, 2012). If a population of cortically projecting axons or a subset of cortical neurons can be synchronously stimulated with transcranial magnetic stimulation during relevant behaviors and sensory inputs (Frantseva et al., 2008; Thabit et al., 2010; Zeller et al., 2010), it might be possible to improve cognitive and behavioral abnormalities in the early stages of diseases featuring impaired myelination.

ACKNOWLEDGMENTS

We thank V. Jayaraman, R. Kerr, D. Kim, L. Looger, and K. Svoboda of the GENIE Project at Janelia Farm Research Campus (HHMI) for providing rAAV2/1-CAG-flex-GCaMP6f and K. Deisseroth at Stanforde University for providing rAAV2/1-Syn-ChR2 (H134R)-EYFP. rAAV2/1-Syn-GCaMP3 was synthesized and purified by Takashi Okada (Nippon Medical School, Japan) with the AAV2/1 helper plasmid (J.M. Wilson, University of Pennsylvania). This work was supported by Grants-in-Aid for Scientific Research on Innovative Areas (15H01300, 16H01346, 17H05747, 19H04753, 19H05219, and 25110732 to H.W.; 22115005 and 17H06309 to M.M.); by Grants-in-Aid for Young Scientists (A) (26710004 to H.W.); Grant-in-Aid for Scientific Research (B) (18H02598 to H.W.); by Grants-in-Aid for Scientific Research (23300148 to M.M.) from the Ministry of Education, Culture, Sports, Science, and Technology (MEXT), Japan; by AMED (JP17dm0107053 to M.M.) and by JST CREST Grant Number JPMJCR1755, Japan.

CONFLICT OF INTEREST

The authors have no financial conflict of interest.

AUTHORS CONTRIBUTIONS

D.K., H.W., N.M., J.N., and M.M. designed the research. D.K., H.W., P.R.L., Y.T., R. O., Y. T. and S. S. performed the experiments with advice from Y.H.T., Y.M., A.J.M., N.T., and K.I. R.H. developed the task apparatus, and Y.R.T. developed the scripts for motion correction and ROI extraction. D.K. and H.W. analyzed the data. D.K., H.W., R.D.F., and M.M. wrote the manuscript with comments from all other authors.

ORCID

Hiroaki Wake https://orcid.org/0000-0002-8543-4590
Kazuhiro Ikenaka https://orcid.org/0000-0002-2983-2498
R. Douglas Fields https://orcid.org/0000-0001-8627-0447

REFERENCES

Amlien, I. K., & Fjell, A. M. (2014). Diffusion tensor imaging of white matter degeneration in Alzheimer's disease and mild cognitive impairment. *Neuroscience*, *276*, 206–215.

Back, S. A., Kroenke, C. D., Sherman, L. S., Lawrence, G., Gong, X., Taber, E. N., … Montine, T. J. (2011). White matter lesions defined by diffusion tensor imaging in older adults. *Annals of Neurology*, *70*, 465–476.

Balleine, B. W., & O'Doherty, J. P. (2010). Human and rodent homologies in action control: Corticostriatal determinants of goal-directed and habitual action. *Neuropsychopharmacology*, *35*, 48–69.

Bando, Y., Takakusaki, K., Ito, S., Terayama, R., Kashiwayanagi, M., & Yoshida, S. (2008). Differential changes in axonal conduction following CNS demyelination in two mouse models. *European Journal of Neuroscience*, *28*, 1731–1742.

Barres, B. A., & Raff, M. C. (1993). Proliferation of oligodendrocyte precursor cells depends on electrical activity in axons. *Nature*, *361*, 258–260.

Bennett, I. J., & Madden, D. J. (2014). Disconnected aging: Cerebral white matter integrity and age-related differences in cognition. *Neuroscience*, *276*, 187–205.

Bosch-Bouju, C., Hyland, B. I., & Parr-Brownlie, L. C. (2013). Motor thalamus integration of cortical, cerebellar and basal ganglia information: Implications for normal and parkinsonian conditions. *Frontiers in Computational Neuroscience*, *7*, 163.

Busche, M. A., Eichhoff, G., Adelsberger, H., Abramowski, D., Wiederhold, K. H., Haass, C., … Garaschuk, O. (2008). Clusters of hyperactive neurons near amyloid plaques in a mouse model of Alzheimer's disease. *Science*, *321*, 1686–1689.

Castro-Alamancos, M. A. (2013). The motor cortex: A network tuned to 7-14 Hz. *Frontiers in Neural Circuits*, *7*, 21.

Chehrehasa, F., Meedeniya, A. C., Dwyer, P., Abrahamsen, G., & Mackay-Sim, A. (2009). EdU, a new thymidine analogue for labelling proliferating cells in the nervous system. *Journal of Neuroscience Methods*, *177*, 122–130.

Chen, T. W., Wardill, T. J., Sun, Y., Pulver, S. R., Renninger, S. L., Baohan, A., … Kim, D. S. (2013). Ultrasensitive fluorescent proteins for imaging neuronal activity. *Nature*, *499*, 295–300.

Ciocchi, S., Passecker, J., Malagon-Vina, H., Mikus, N., & Klausberger, T. (2015). Brain computation. Selective information routing by ventral hippocampal CA1 projection neurons. *Science*, *348*, 560–563.

Costa, R. M., Cohen, D., & Nicolelis, M. A. (2004). Differential corticostriatal plasticity during fast and slow motor skill learning in mice. *Current Biology*, *14*, 1124–1134.

Doyon, J., & Benali, H. (2005). Reorganization and plasticity in the adult brain during learning of motor skills. *Current Opinion in Neurobiology*, *15*, 161–167.

Emery, B. (2010). Regulation of oligodendrocyte differentiation and myelination. *Science*, *330*, 779–782.

Eto, K., Wake, H., Watanabe, M., Ishibashi, H., Noda, M., Yanagawa, Y., & Nabekura, J. (2011). Inter-regional contribution of enhanced activity of the primary somatosensory cortex to the anterior cingulate cortex accelerates chronic pain behavior. *Journal of Neuroscience*, *31*, 7631–7636.

Feldman, D. E. (2012). The spike-timing dependence of plasticity. *Neuron*, *75*, 556–571.

Fields, R. D. (2008). White matter in learning, cognition and psychiatric disorders. *Trends in Neurosciences*, *31*, 361–370.

Frantseva, M. V., Fitzgerald, P. B., Chen, R., Moller, B., Daigle, M., & Daskalakis, Z. J. (2008). Evidence for impaired long-term potentiation in schizophrenia and its relationship to motor skill learning. *Cerebral Cortex*, *18*, 990–996.

Gibson, E. M., Purger, D., Mount, C. W., Goldstein, A. K., Lin, G. L., Wood, L. S., … Monje, M. (2014). Neuronal activity promotes oligodendrogenesis and adaptive myelination in the mammalian brain. *Science*, *344*, 1252304.

Goncalves, J. T., Anstey, J. E., Golshani, P., & Portera-Cailliau, C. (2013). Circuit level defects in the developing neocortex of fragile X mice. *Nature Neuroscience*, *16*, 903–909.

Hakak, Y., Walker, J. R., Li, C., Wong, W. H., Davis, K. L., Buxbaum, J. D., … Fienberg, A. A. (2001). Genome-wide expression analysis reveals dysregulation of myelination-related genes in chronic schizophrenia. *Proceedings of the National Academy of Sciences of the United States of America*, *98*, 4746–4751.

Hines, J. H., Ravanelli, A. M., Schwindt, R., Scott, E. K., & Appel, B. (2015). Neuronal activity biases axon selection for myelination in vivo. *Nature Neuroscience*, *18*, 683–689.

Hira, R., Ohkubo, F., Ozawa, K., Isomura, Y., Kitamura, K., Kano, M., … Matsuzaki, M. (2013). Spatiotemporal dynamics of functional clusters of neurons in the mouse motor cortex during a voluntary movement. *Journal of Neuroscience*, *33*, 1377–1390.

Hooks, B. M., Mao, T., Gutnisky, D. A., Yamawaki, N., Svoboda, K., & Shepherd, G. M. (2013). Organization of cortical and thalamic input to pyramidal neurons in mouse motor cortex. *Journal of Neuroscience*, *33*, 748–760.

Huber, D., Gutnisky, D. A., Peron, S., O'Connor, D. H., Wiegert, J. S., Tian, L., … Svoboda, K. (2012). Multiple dynamic representations in the motor cortex during sensorimotor learning. *Nature*, *484*, 473–478.

Kagawa, T., Ikenaka, K., Inoue, Y., Kuriyama, S., Tsujii, T., Nakao, J., … Mikoshiba, K. (1994). Glial cell degeneration and hypomyelination caused by overexpression of myelin proteolipid protein gene. *Neuron*, *13*, 427–442.

Kimura, F., & Itami, C. (2009). Myelination and isochronicity in neural networks. *Frontiers in Neuroanatomy*, *3*, 12.

Lee, P. R., Cohen, J. E., Tendi, E. A., Farrer, R., DE Vries, G. H., Becker, K. G. & Fields, R. D. (2004). Transcriptional profiling in an MPNST-derived cell line and normal human Schwann cells. *Neuron Glia Biology*, *1*, 135–147.

Li, Q., Brus-Ramer, M., Martin, J. H., & McDonald, J. W. (2010). Electrical stimulation of the medullary pyramid promotes proliferation and differentiation of oligodendrocyte progenitor cells in the corticospinal tract of the adult rat. *Neuroscience Letters*, *479*, 128–133.

Liu, J., Dietz, K., DeLoyht, J. M., Pedre, X., Kelkar, D., Kaur, J., … Casaccia, P. (2012). Impaired adult myelination in the prefrontal cortex of socially isolated mice. *Nature Neuroscience*, *15*, 1621–1623.

Makino, H., Hwang, E. J., Hedrick, N. G., & Komiyama, T. (2016). Circuit mechanisms of sensorimotor learning. *Neuron*, *92*, 705–721.

Makinodan, M., Rosen, K. M., Ito, S., & Corfas, G. (2012). A critical period for social experience-dependent oligodendrocyte maturation and myelination. *Science*, *337*, 1357–1360.

Martini, R., & Schachner, M. (1997). Molecular bases of myelin formation as revealed by investigations on mice deficient in glial cell surface molecules. *Glia*, *19*, 298–310.

Masamizu, Y., Tanaka, Y. R., Tanaka, Y. H., Hira, R., Ohkubo, F., Kitamura, K., … Matsuzaki, M. (2014). Two distinct layer-specific dynamics of cortical ensembles during learning of a motor task. *Nature Neuroscience*, *17*, 987–994.

McKenzie, I. A., Ohayon, D., Li, H., de Faria, J. P., Emery, B., Tohyama, K., & Richardson, W. D. (2014). Motor skill learning requires active central myelination. *Science*, *346*, 318–322.

Mensch, S., Baraban, M., Almeida, R., Czopka, T., Ausborn, J., El Manira, A., & Lyons, D. A. (2015). Synaptic vesicle release regulates myelin sheath number of individual oligodendrocytes in vivo. *Nature Neuroscience*, *18*, 628–630.

Miall, R. C., Price, S., Mason, R., Passingham, R. E., Winter, J. L., & Stein, J. F. (1998). Microstimulation of movements from cerebellar-receiving, but not pallidal-receiving areas of the macaque thalamus under ketamine anaesthesia. *Experimental Brain Research*, *123*, 387–396.

Moldakarimov, S., Bazhenov, M., & Sejnowski, T. J. (2015). Feedback stabilizes propagation of synchronous spiking in cortical neural networks. *Proceedings of the National Academy of Sciences of the United States of America*, *112*, 2545–2550.

Nave, K. A. (2010). Myelination and support of axonal integrity by glia. *Nature*, *468*, 244–252.

Nave, K. A., & Ehrenreich, H. (2014). Myelination and oligodendrocyte functions in psychiatric diseases. *JAMA Psychiatry*, *71*, 582–584.

O'Connor, D. H., Peron, S. P., Huber, D., & Svoboda, K. (2010). Neural activity in barrel cortex underlying vibrissa-based object localization in mice. *Neuron*, *67*, 1048–1061.

Pajevic, S., Basser, P. J., & Fields, R. D. (2014). Role of myelin plasticity in oscillations and synchrony of neuronal activity. *Neuroscience*, *276*, 135–147.

Peters, A. J., Chen, S. X., & Komiyama, T. (2014). Emergence of reproducible spatiotemporal activity during motor learning. *Nature*, *510*, 263–267.

Roelfsema, P. R., Engel, A. K., Konig, P., & Singer, W. (1997). Visuomotor integration is associated with zero time-lag synchronization among

cortical areas. *Nature*, *385*, 157–161.

Salami, M., Itami, C., Tsumoto, T., & Kimura, F. (2003). Change of conduction velocity by regional myelination yields constant latency irrespective of distance between thalamus and cortex. *Proceedings of the National Academy of Sciences of the United States of America*, *100*, 6174–6179.

Sampaio-Baptista, C., Khrapitchev, A. A., Foxley, S., Schlagheck, T., Scholz, J., Jbabdi, S., … Johansen-Berg, H. (2013). Motor skill learning induces changes in white matter microstructure and myelination. *Journal of Neuroscience*, *33*, 19499–19503.

Saugier-Veber, P., Munnich, A., Bonneau, D., Rozet, J. M., Le Merrer, M., Gil, R., & Boespflug-Tanguy, O. (1994). X-linked spastic paraplegia and Pelizaeus-Merzbacher disease are allelic disorders at the proteolipid protein locus. *Nature Genetics*, *6*, 257–262.

Scholz, J., Klein, M. C., Behrens, T. E., & Johansen-Berg, H. (2009). Training induces changes in white-matter architecture. *Nature Neuroscience*, *12*, 1370–1371.

Schulman, J. J., Cancro, R., Lowe, S., Lu, F., Walton, K. D., & Llinas, R. R. (2011). Imaging of thalamocortical dysrhythmia in neuropsychiatry. *Frontiers in Human Neuroscience*, *5*, *69*.

Shadmehr, R., & Krakauer, J. W. (2008). A computational neuroanatomy for motor control. *Experimental Brain Research*, *185*, 359–381.

Shimizu, T., Tanaka, K. F., Takebayashi, H., Higashi, M., Wisesmith, W., Ono, K., … Ikenaka, K. (2013). Olig2-lineage cells preferentially differentiate into oligodendrocytes but their processes degenerate at the chronic demyelinating stage of proteolipid protein-overexpressing mouse. *Journal of Neuroscience Research*, *91*, 178–186.

Shine, H. D., Readhead, C., Popko, B., Hood, L., & Sidman, R. L. (1992). Morphometric analysis of normal, mutant, and transgenic CNS: Correlation of myelin basic protein expression to myelinogenesis. *Journal of Neurochemistry*, *58*, 342–349.

Tanahira, C., Higo, S., Watanabe, K., Tomioka, R., Ebihara, S., Kaneko, T., & Tamamaki, N. (2009). Parvalbumin neurons in the forebrain as revealed by parvalbumin-Cre transgenic mice. *Neuroscience Research*, *63*, 213–223.

Tanaka, H., Ikenaka, K., & Isa, T. (2006). Electrophysiological abnormalities precede apparent histological demyelination in the central nervous system of mice overexpressing proteolipid protein. *Journal of Neuroscience Research*, *84*, 1206–1216.

Tanaka, H., Ma, J., Tanaka, K. F., Takao, K., Komada, M., Tanda, K., … Ikenaka, K. (2009). Mice with altered myelin proteolipid protein gene expression display cognitive deficits accompanied by abnormal neuron-glia interactions and decreased conduction velocities. *Journal of Neuroscience*, *29*, 8363–8371.

Tanaka, Y. H., Tanaka, Y. R., Kondo, M., Terada, S. I., Kawaguchi, Y., & Matsuzaki, M. (2018). Thalamocortical axonal activity in motor cortex exhibits layer-specific dynamics during motor learning. *Neuron*, *100*, 244–258.e212.

Tennant, K. A., Taylor, S. L., White, E. R., & Brown, C. E. (2017). Optogenetic rewiring of thalamocortical circuits to restore function in the stroke injured brain. *Nature Communications*, *8*, 15879.

Thabit, M. N., Ueki, Y., Koganemaru, S., Fawi, G., Fukuyama, H., & Mima, T. (2010). Movement-related cortical stimulation can induce human motor plasticity. *Journal of Neuroscience*, *30*, 11529–11536.

Tian, L., Hires, S. A., Mao, T., Huber, D., Chiappe, M. E., Chalasani, S. H., … Looger, L. L. (2009). Imaging neural activity in worms, flies and mice with improved GCaMP calcium indicators. *Nature Methods*, *6*, 875–881.

Veniero, D., Ponzo, V., & Koch, G. (2013). Paired associative stimulation enforces the communication between interconnected areas. *Journal of Neuroscience*, *33*, 13773–13783.

Wake, H., Lee, P. R., & Fields, R. D. (2011). Control of local protein synthesis and initial events in myelination by action potentials. *Science*, *333*, 1647–1651.

Wake, H., Ortiz, F. C., Woo, D. H., Lee, P. R., Angulo, M. C., & Fields, R. D. (2015). Nonsynaptic junctions on myelinating glia promote preferential myelination of electrically active axons. *Nature Communications*, *6*, 7844.

Whitford, T. J., Ford, J. M., Mathalon, D. H., Kubicki, M., & Shenton, M. E. (2012). Schizophrenia, myelination, and delayed corollary discharges: A hypothesis. *Schizophrenia Bulletin*, *38*, 486–494.

Xiao, L., Ohayon, D., McKenzie, I. A., Sinclair-Wilson, A., Wright, J. L., Fudge, A. D., … Richardson, W. D. (2016). Rapid production of new oligodendrocytes is required in the earliest stages of motor-skill learning. *Nature Neuroscience*, *19*, 1210–1217.

Yin, H. H., Mulcare, S. P., Hilario, M. R., Clouse, E., Holloway, T., Davis, M. I., … Costa, R. M. (2009). Dynamic reorganization of striatal circuits during the acquisition and consolidation of a skill. *Nature Neuroscience*, *12*, 333–341.

Zatorre, R. J., Fields, R. D., & Johansen-Berg, H. (2012). Plasticity in gray and white: Neuroimaging changes in brain structure during learning. *Nature Neuroscience*, *15*, 528–536.

Zeller, D., aufm Kampe, K., Biller, A., Stefan, K., Gentner, R., Schutz, A., … Classen, J. (2010). Rapid-onset central motor plasticity in multiple sclerosis. *Neurology*, *74*, 728–735.

Zhang, W., Peterson, M., Beyer, B., Frankel, W. N., & Zhang, Z. W. (2014). Loss of MeCP2 from forebrain excitatory neurons leads to cortical hyperexcitation and seizures. *Journal of Neuroscience*, *34*, 2754–2763.

SUPPORTING INFORMATION

Additional supporting information may be found online in the Supporting Information section at the end of this article.

How to cite this article: Kato D, Wake H, Lee PR, et al. Motor learning requires myelination to reduce asynchrony and spontaneity in neural activity. *Glia*. 2020;68:193–210. https://doi.org/10.1002/glia.23713